

Active deformation and Plio-Pleistocene fluvial reorganization of the western Kura Fold-Thrust Belt, Georgia: implications for the evolution of the Greater Caucasus mountains and seismic hazard

Journal:	<i>Geological Magazine</i>
Manuscript ID	Draft
Manuscript Type:	Original Article
Date Submitted by the Author:	n/a
Complete List of Authors:	Sukhishvili, Lasha; Ilia State University, Institute of Earth Sciences and NSMC Forte, Adam; Louisiana State University, Department of Geology & Geophysics Merebashvili, Giorgi; Ilia State University, Institute of Earth Sciences and NSMC Leonard, Joel; Arizona State University, School of Earth and Space Exploration Whipple, Kelin; Arizona State University, School of Earth and Space Exploration Javakhishvili, Zurab; Ilia State University, Institute of Earth Sciences and NSMC Heimsath, Arjun; Arizona State University, School of Earth and Space Exploration Godoladze, Tea; Ilia State University, Institute of Earth Sciences and NSMC
Keywords:	Tectonic geomorphology, Alazani basin, Gombori range, Paleocurrent analysis, Burial age dating, Greater Caucasus, Kura Fold-Thrust Belt

1
2
3 1 **Active deformation and Plio-Pleistocene fluvial reorganization of the western Kura Fold-**
4
5
6 2 **Thrust Belt, Georgia: implications for the evolution of the Greater Caucasus mountains and**
7
8 3 **seismic hazard**
9

10
11 4
12
13 5 Manuscript category: Tectonics and Structural Geology
14
15 6

16
17
18 7 Lasha Sukhishvili¹, Adam M. Forte², Giorgi Merebashvili¹, Joel Leonard³, Kelin X. Whipple³, Zurab
19
20 8 Javakhishvili¹, Arjun Heimsath³, Tea Godoladze¹
21
22

23 9 ¹Institute of Earth Sciences and National Seismic Monitoring Centre, Ilia State University, Tbilisi,
24
25
26 10 Georgia
27
28

29 11 ²Department of Geology & Geophysics, Louisiana State University, Baton Rouge, LA, USA
30
31

32 12 ³School of Earth and Space Exploration, Arizona State University, Tempe, AZ, USA
33
34
35
36 13

37
38 14 Corresponding author: Lasha Sukhishvili
39
40

41 15 Email: lasha.sukhishvili@iliauni.edu.ge
42
43
44
45
46 16
47 17
48
49
50 18
51
52
53
54
55
56
57
58
59
60

1
2
3 19 **Abstract**
4

5
6 20 Since the Plio-Pleistocene, southward migration of shortening in the eastern part of the Greater
7
8 21 Caucasus (GC) into the Kura foreland basin has progressively formed the Kura-Fold Thrust belt
9
10 22 (KFTB) and Alazani piggyback basin, which separates the KFTB from the GC. Previous work
11
12
13 23 argued for an eastward propagation of the KFTB, implying that the western portion in Georgia is
14
15 24 the oldest, but this hypothesis was based on coarse geologic maps and speculative ages for
16
17
18 25 units within the KFTB. Here we investigate this hypothesis and focus on the Gombori Range
19
20 26 (GR), which defines NW edge of the belt. Previous work divided the sediments of northern flank
21
22
23 27 of the range into three facies. The rock types in the older and middle facies suggest a GC source
24
25 28 provenance, despite the modern drainage network in the NE GR, which is dominated by NE
26
27
28 29 flowing rivers.

29
30
31 30 Paleocurrent analyses of the alluvial conglomerates of the oldest and youngest syntectonic
32
33 31 units indicate a switch from dominantly SW directed paleocurrents in the oldest unit to
34
35 32 paleocurrents more similar to the modern drainage network in the youngest unit. A single
36
37
38 33 successful ^{26}Al - ^{10}Be burial date indicates these syntectonic sediments are 1 ± 1 Ma, which while
39
40
41 34 not a precise age, is consistent with original mapping suggesting these sediments are Akchagyl-
42
43 35 Apsheron (2.7-0.88 Ma) age. Tectonic geomorphologic analyses indicate that western GR is the
44
45 36 most active. Given its close proximity to the capital city of Tbilisi, this suggests that active
46
47
48 37 structures within the Gombori range pose seismic hazard to this city of 1.2 million people.

49
50
51 38
52
53
54
55
56
57
58
59
60

1. Introduction and Motivation

The Kura Fold-Thrust belt (KFTB) is located between the Greater Caucasus (GC) and Lesser Caucasus Mountains and represents a major structural system within this region, accommodating shortening between these two orogenic systems (e.g. Forte *et al.* 2010; Forte *et al.* 2013). Closure of the Greater Caucasus back-arc basin in the late Miocene and the transition from subduction to collision in the Pliocene, resulted in a fast exhumation phase of the Greater Caucasus (Avdeev & Niemi 2011), however the exact timing of collision along-strike remains controversial (e.g. Cowgill *et al.* 2016; Vincent *et al.* 2016). Since the Plio-Pleistocene, much of the shortening in the eastern half of the Greater Caucasus has propagated southward, into the Kura foreland basin, and formed the KFTB (**Error! Reference source not found.**). Since initiation of deformation within the KFTB, it has accommodated approximately half of total Arabia-Eurasia convergence at the longitude of the eastern GC (Forte *et al.* 2013). Geodetic measurements indicate that there is an along-strike, eastward increasing velocity gradient between the Greater and Lesser Caucasus, with approximately 8 mm/yr of expected convergence between the two ranges at the longitude of the center of the KFTB (Reilinger *et al.* 2006). However, while efforts are ongoing to densify the GPS network throughout the KFTB, at present station coverage is not sufficient to perform further analyses. By analyzing large twentieth century earthquakes in eastern Turkey and the Caucasus and expected Arabia-Eurasia motion, Jackson & Mckenzie (1988) and Jackson (1992) hypothesized that the Caucasus must be deforming mostly aseismically, either by creep on faults or by folding. It might be expected that shortening, especially by folding, of thick, possibly overpressurized, sediments, should occur without generating major earthquakes, even if folding were to occur above buried

1
2
3 61 (blind) thrust or reverse faults (Jackson, 1992). Nevertheless, from the eastern domain of the
4
5
6 62 KFTB in Azerbaijan, there are strong indications that the Kura fold-thrust belt is actively
7
8 63 deforming (Forte *et al.* 2010 and 2013; Mosar *et al.* 2010) and thus the potential seismic
9
10 64 hazard within the fold-thrust belt may be underestimated. There are several Mw 5-5.4
11
12
13 65 earthquakes within the KFTB area in the Complete Catalogue of Instrumental Seismicity for
14
15 66 Georgia (Onur, *et al.* 2019). The earthquake data indicates a south-dipping low-angle thrust
16
17
18 67 under the Gombori ridge, which is consistent with geologic observations throughout the KFTB
19
20 68 (Forte *et al.* 2010, 2013; Adamia *et al.* 2010, 2011) The strike of the fault plane of a M 5.4 event
21
22 69 (27.11.1997) was approximately east-west (Tan & Taymaz, 2006), also consistent with the
23
24
25 70 structural geometries within the KFTB (Figure 2). However, detailed paleoseismic studies have
26
27
28 71 never been conducted in the region, leaving significant uncertainties about the seismic hazard.
29
30
31 72 Previous work on the KFTB noted that there is more elevated topography (measured with
32
33 73 respect to the adjacent basins), cross-strike width, and older structures exposed in the western
34
35
36 74 part of the belt. Forte *et al.* (2010) argued this pattern could be caused by an eastward
37
38 75 decrease of total shortening, timing of initiation, or combination thereof. According to *Alania et*
39
40 76 *al.* (2017), the formation of Kakheta Ridge (located at the western part of KFTB, here referred to
41
42
43 77 as the Gombori Range), took place in the Pliocene, while estimates of the initiation of
44
45 78 deformation within the eastern segment of the belt lie between 1.8-1.5 Ma by Forte *et al.*
46
47
48 79 (2013), though more recent dating of Eastern KFTB stratigraphy suggests deformation may have
49
50 80 initiated closer to 2.2-2.0 Ma (e.g. Lazarev *et al.* 2019). This is consistent with the idea first
51
52
53 81 proposed by Forte *et al.* (2010) that deformation started in the western KFTB and propagated
54
55 82 eastward. While these independent studies show a consistent eastward propagating pattern of
56
57
58
59
60

1
2
3 83 deformation and deformation initiation age along-strike within the KFTB, this is complicated by
4
5
6 84 the fact that there is a better understanding of stratigraphy and the deformation pattern of the
7
8 85 central and eastern part of KFTB, whereas much remains uncertain about the western domain.
9

10
11 86 Additional evidence of along-strike variation in structural history is interpretable from the
12
13
14 87 topography and comparisons between the modern drainage network and the paleo-drainage
15
16 88 network of the KFTB as reconstructed from alluvial stratigraphy. Specifically, in the eastern
17
18 89 KFTB, south flowing rivers sourced from the GC still cross the KFTB, but west of where the
19
20
21 90 Alazani river enters the KFTB, no south flowing river from the GC crosses the KFTB (Figure 1). It
22
23 91 is a reasonable expectation that prior to the development of the KFTB and during some portion
24
25
26 92 of the deposition of pre and syntectonic alluvial sediments now exposed within the KFTB, some
27
28 93 GC-sourced rivers did make it to, or through, the KFTB. Such drainage reorganizations during the
29
30
31 94 progressive growth of fold belts is observed in both natural examples (e.g. Bretis *et al.* 2011; Burbank *et*
32
33 95 *al.* 1996; Davis *et al.* 2005; Delcaillau *et al.* 1998; Delcaillau *et al.* 2001; Delcaillau *et al.* 2006; Keller *et al.*
34
35 96 1999; Lawton *et al.* 1994) and experiments (e.g. Champel *et al.* 2002; (Douglass and Schmeeckle 2007).
36
37 97 The timing of drainage reorganization in the western KFTB would provide an important constraint on the
38
39 98 structural and topographic evolution of this portion of the KFTB and thus help constrain the along-strike
40
41
42 99 evolution of the KFTB overall.
43

44
45 100 To investigate how compatible the geology of the western segment of the KFTB is to the above
46
47 101 proposed models, we applied quantitative tectonic geomorphologic approaches, ^{26}Al - ^{10}Be
48
49 102 burial dating, and paleocurrent analyses within the Gombori Range.
50

51
52
53 103
54
55
56
57
58
59
60

104 2. Stratigraphic background

105 The Gombori range, which is the highest relief part of the KFTB and defines the NW edge of the
106 belt, is built by deformed lower and upper Cretaceous, Eocene and Oligocene, Miocene, Plio-
107 Pleistocene and Quaternary period rocks (Figure 3. *Stratigraphy of the Gombori range compiled*
108 *after (Buleishvili, 1974), (Zedginidze et al. 1971), (Kereselidze, 1950), (Sidorenko & Gamkrelidze,*
109 *1964), (Buachidze et al. 1950)*). Here we focus exclusively on the Plio-Pleistocene sediments of
110 the Gombori range.

111 Previous work has described the Plio-Pleistocene sediments of the Gombori range as a part of
112 the Akchagyl-Apsheron regional stages and are collectively described as the Alazani series.

113 Within the Caspian Sea region and its subbasins, the Akchagylian regional stage corresponds to
114 the late Pliocene epoch (Jones & Simmons, 1996; Krijgsman *et al.* 2018). The Akchagylian
115 represents a series of large transgressions, which temporarily re-established marine
116 connections between Caspian Sea and world ocean (Jones & Simmons 1996; Forte & Cowgill,
117 2013; Van Baak *et al.* 2019). The Akchagylian sediments are broadly considered as being
118 deposited in a marine environment (Jones & Simmons 1996), but there are continental facieses
119 of Akchagylian stage within the eastern (Forte *et al.* 2015) central and western KFTB as well
120 (Chkhikvadze *et al.* 2000; Alania *et al.* 2017; Sidorenko & Gamkrelidze, 1964). The Apsheronian
121 stage, which overlies the Akchagylian, is essentially regressive in character and corresponds to
122 lower and middle Pleistocene (Jones & Simmons, 1996; Krijgsman *et al.* 2018). It generally
123 represents shallow marine and continental deposits, but within the Gombori range,
124 Apsheronian sediments are considered part of the Alazani series, which has previously been
125 interpreted as being deposited in a terrestrial environment (Sidorenko & Gamkrelidze, 1964).

1
2
3 126 The maximum thickness of the Alazani series at the NE slope of Gombori range is ca. 1800m
4
5
6 127 (Sidorenko & Gamkrelidze, 1964) between catchments 7 (riv. Kisiskhevi) and 12 (riv.
7
8 128 Papriskhevi) (Figure 3) (Buachidze *et al.* 1950; Buleishvili, 1974) and thins to ca. 1400m along
9
10 129 the SW slope of the Gombori range (Sidorenko & Gamkrelidze, 1964).

13
14 130 Three facies, Al₁, Al₂, and Al₃ have been previously defined within the Alazani series. There is an
15
16 131 angular unconformity at the base of the Alazani series between it and the older Neogene,
17
18 132 Paleogene and Cretaceous sediments. Angular unconformities are also present between all of
19
20
21 133 the Alazani series facies.

22
23
24 134 The lower Al₁ is represented by well-consolidated conglomerates and cobbles with 0.2-1.5m
25
26 135 thick lenses of loams and clays. The lowest boundary of the Al₁ facies is marked by a bluish
27
28 136 color conglomerate (Figure 4). The longest axis of cobbles within this conglomeratic interval
29
30
31 137 averages between 10-15cm. Sandstone, schist, limestone and marl clasts are the dominant rock
32
33
34 138 types of cobbles and conglomerates within the Al₁ facies. Some of these rock types here (e.g.
35
36 139 schists) are typical for the Greater Caucasus and suggest that these sediments are sourced
37
38
39 140 broadly from the north (Buachidze *et al.* 1950; Sidorenko & Gamkrelidze, 1964), but detailed
40
41 141 provenance analyses of these sediments are yet to be performed. The thickness of the Al₁ facies
42
43
44 142 is ca. 700m. The Al₁ layers broadly define the Gombori range as an anticlinorium, with Al₁ layers
45
46 143 dominantly north dipping at ca. 50-60° along the NE slope and southeast dipping at ca. 20-45°
47
48
49 144 along the southern slope. Surface elevation of exposures of the lower boundary of Al₁ facies
50
51 145 within Gombori range is at 481m, but as it is challenging to distinguish between the lower Al₁
52
53 146 and upper Al₃ facies in the field, and thus a clear upper limit for Al₁ facies are not estimated yet,
54
55
56 147 but it might reach to 1991m.

1
2
3 148 The overlying Al_2 facies is mostly dominated by loam and clay, but small amounts of cobbles
4
5
6 149 and conglomerates are also present. As in the Al_1 facies, the rock types in this facies are also
7
8 150 suggestive of a Greater Caucasus source (Buachidze *et al.* 1952). The maximum thickness of this
9
10 151 facies is ca. 500m at catchment 6 and gradually decreases to 50m to South-Eastern direction
11
12
13 152 (Buachidze *et al.* 1952). In the northern slope of the Gombori, the Al_2 facies dip to the NE, but
14
15 153 at shallower angles with respect to the underlying Al_1 facies, with average dips in Al_2 facies
16
17 154 rocks being ca. 20° - 30° . This facies contains a thin layer of volcanic ash (Figure 5). The surface
18
19 155 elevation of Al_2 facies exposures within Gombori range varies between 448 and 1569m.
20
21
22

23 156 The upper Al_3 facies is dominantly composed of conglomerates with minor interbeds of loams
24
25 157 and clays. According to some reports (e.g. Kereselidze, 1950) another volcanic ash layer of 0.4
26
27 158 m thickness is traceable within loamy layer of catchments 6 and 7, but we did not observe this
28
29 159 ash layer in the field. The thickness of this facies is between 150-250m. Layers within the Al_3
30
31 160 facies exposed along the NE edge of the Gombori dip shallowly to the NE at 5° - 15° . The surface
32
33 161 elevation of exposures of Al_3 facies within the Gombori range varies between 390 – 1210m.
34
35
36 162 There also exist isolated packages of conglomerate higher in the Gombori range that are
37
38 163 unconformable with the underlying, older stratigraphy, and are likely exposures of the Alazani
39
40 164 series. These exposures may be associated with the Al_3 facies, but could also be associated with
41
42 165 the Al_1 facies as outside of their stratigraphic context, it is difficult to distinguish between these
43
44 166 two facies.
45
46
47
48
49
50

51 167
52
53
54
55
56
57
58
59
60

1
2
3 168 **3. Methods**
4

5
6 169 **3.a. Paleocurrent analyses**
7

8 170 Modern rivers draining the NE slopes of the Gombori range flow NE and drain into the Alazani
9
10 171 valley, but archival data of geological reports (Buachidze *et al.* 1950; Buachidze *et al.* 1952)
11
12 172 suggests that the alluvial sediments of the Alazani series contain rock types typical for the
13
14 173 Greater Caucasus, suggesting a southward flow of rivers during the deposition of at least some
15
16 174 of the sediments.
17
18

19
20
21 175 Alluvial channels are very sensitive to active tectonics and adjust to vertical deformation or
22
23 176 base level change by channel modification (Merritts *et al.* 1994). Research on fluvial terraces (as
24
25 177 abandoned floodplains) using gravel or pebble imbrication, is one of the reliable indicators of
26
27 178 paleocurrent in coarse grained deposits and can shed light on tectonic evolution of the site
28
29 179 (Miao *et al.* 2008). The direction of imbrication of oblate clasts in a conglomerate can be used
30
31 180 to indicate the direction of the flow that deposited the gravel (Nichols, 2009).
32
33

34
35
36 181 Exposures of Alazani series sediments in the walls of canyons along the main stem rivers of
37
38 182 catchments 7 and 11 were selected for paleocurrent analyses. A total of 265 clasts were
39
40 183 measured from four sites of Al₁ and Al₃ facies of both catchments. In this study, we measured
41
42 184 the orientation of the clast imbrication with a Brunton compass and performed unfolding and
43
44 185 further processing using Stereonet 10 software (Allmendinger *et al.* 2011). We performed this
45
46 186 paleocurrent analysis to specifically test whether there was evidence of flow reversal and/or
47
48 187 drainage reorganization during the deposition of the potentially syntectonic Alazani series
49
50 188 sediments.
51
52
53
54
55
56
57
58
59
60

189 **3.b. Tectonic geomorphology**

190 Topography reflects the balance between rock uplift, driven by tectonics, and erosional and
191 depositional processes modulated by climate and lithology. With careful consideration of
192 potential climatic and lithological complications, quantitative geomorphic analyses can
193 constrain relative differences in rates of rock uplift, and thus inform our understanding of
194 tectonics (e.g., Kirby & Whipple, 2001; Wobus *et al.* 2006; Dibiase *et al.* 2010; Kirby & Whipple
195 2012; Whittaker, 2012; Whittaker & Boulton 2012; Rossi *et al.* 2017; Gallen & Wegmann 2017).
196 Importantly, in the absence of other data, e.g. dense geodetic networks and/or long-term and
197 complete seismic and paleoseismic records, tectonic geomorphology can also be useful in
198 highlighting areas of active tectonics and potential seismic hazard (e.g. Kirby *et al.* 2008).

199 To evaluate the activity within the western end of the KFTB, we selected the twelve largest
200 catchments (14-108 km²) along the northern slope of Gombori range and calculated several
201 morphometric parameters using TAK (Forte & Whipple, 2018), TopoToolbox (Schwanghart &
202 Scherler, 2014), and QGIS using a digital elevation model (DEM) acquired through the ALOS
203 AW3D30. The DEM is produced by the Japan Aerospace Exploration Agency (JAXA) and has a
204 horizontal resolution of ~30m (available from [http://www.eorc.
205 jaxa.jp/ALOS/en/aw3d30/index.htm](http://www.eorc.jaxa.jp/ALOS/en/aw3d30/index.htm)). The AW3D30 DEM dataset was generated based on the
206 0.15-arcsec AW3D DEM dataset. Two resampling methods were applied to obtain one pixel
207 value on AW3D30 from 7 by 7 pixels on AW3D. The first one is used the averaging method
208 (Ave), which is simply calculated as an average value from appropriate 49 pixels except for
209 masked out values. Another is the medium method (Med), which is selected a medium height
210 value i.e. 25th height from 49 pixels. If it shows a masked value, same value is kept in AW3D30.

1
2
3 211 The both Ave and Med datasets are contained in individual AW3D30 dataset, which can be
4
5
6 212 downloaded free of charge. AW3D30 Ave DEM has vertical accuracy of 5 m (RMSE) (Tadono *et*
7
8 213 *al.* 2016) using the EGM96 vertical reference frame (JAXA 2017). In this study, the average
9
10 214 dataset is used.

11
12
13
14 215 We attempted to limit our analyses to areas that were bedrock streams, as many of the metrics
15
16 216 were designed for application to bedrock rivers. Thus, we avoid the lower portions of
17
18 217 catchments as these portions of the rivers are likely more alluvial in character and, additionally,
19
20
21 218 are zones of intense agricultural activities and other human modifications.

22
23
24 219 Another important point is the relationship between climate, i.e. precipitation, and tectonics
25
26 220 and how this relationship is reflected in the topography of actively deforming regions, which is
27
28 221 a long-standing debate (e.g. Whipple, 2009). We generally expect that topography may reflect
29
30
31 222 spatial variations in precipitation, so it is important to characterize precipitation as part of a
32
33
34 223 topographic analysis (e.g. Kirby & Whipple, 2012).

35
36
37 224 We use satellite data from the Tropical Rainfall Measurement Mission (TRMM) 3B42 V7
38
39 225 collected from 1998–2017. TRMM dataset contains daily rainfall information recorded in 30km
40
41
42 226 size pixels. TRMM derived rainfall data is well-tested in tectonic geomorphologic studies in
43
44 227 Caucasus (Forte *et al.* 2016), Andes (Bookhagen & Strecker, 2008) and Himalayas (Bookhagen &
45
46 228 Burbank, 2006). **Error! Reference source not found.** shows that all twelve catchments are
47
48
49 229 covered by five TRMM pixels.

50
51
52 230 Similar to climatic influences on topography, lithology and contacts between very different
53
54
55 231 lithologies can produce patterns in topography that may be confused with tectonic signals (e.g.

1
2
3 232 Mitchell & Yanites, 2019). Different lithological units can have different resistances to erosion,
4
5
6 233 which can be a strong control on channel gradient and topography. Lithological contacts and
7
8 234 catchment-dominant rock types were identified to include in tectonic geomorphologic analyses.
9
10 235 To check the correlations between lithological units (including rock properties) and topographic
11
12
13 236 indices we compiled several geological Soviet era geologic maps with new field observations
14
15
16 237 and mapping. For each catchment, we calculated dominant rock types (according to surface
17
18 238 area) to correlate this data to other tectonic geomorphologic proxies.

19
20
21 239 For our quantitative topographic analyses, we calculated the normalized channel steepness
22
23 240 index (K_{sn}), catchment-averaged normalized channel steepness index, total catchment relief,
24
25 241 catchment-averaged hillslope gradient (S_{avg}), catchment-averaged local relief calculated using a
26
27
28 242 1km-radius circle, and drainage area for all selected catchments.

29
30
31 243

34 244 **3.b.1. Channel steepness index**

35
36
37 245 Normalized channel steepness index is an important topographic metric in active ranges (e.g.
38
39 246 Dibiase *et al.* 2010). Despite incomplete understanding of the varied processes contributing to
40
41
42 247 fluvial erosion, the stream profile method has proven an invaluable qualitative tool for
43
44 248 neotectonic investigations. When controlling for differences in precipitation and lithology,
45
46
47 249 empirical observations and simple models of fluvial erosion suggest a positive correlation
48
49 250 between channel gradient and rock uplift rate (e.g. Wobus *et al.* 2006).

50
51
52 251 Typical river longitudinal profiles, for both bedrock and alluvial rivers, are concave and can be
53
54
55 252 described by an empirical power law relationship between slope and area:

1
2
3 253 $S = k_{sn} A^{-\theta}$, and

4
5
6
7
8 254 $k_{sn} = \frac{S}{A^{-\theta}}$

9
10 255 where S is slope, K_{sn} is the normalized channel steepness index, A is the upstream contributing
11
12 256 drainage area, and θ is the channel concavity index (Flint, 1974) Numerous studies indicate
13
14
15 257 that the most channels have uniform concavity regardless of the uplift rate (Snyder *et al.* 2000;
16
17
18 258 Whipple, 2004), because the concavity index (θ) is relatively insensitive to differences in rock
19
20
21 259 uplift rate, climate or substrate lithology at steady-state (provided such differences are uniform
22
23 260 along the length of the channel), while the steepness index (k_s) varies with these factors,
24
25 261 therefore steepness index is a useful metric for tectonic geomorphic studies (Kirby & Whipple,
26
27
28 262 2012).

29
30
31 263 To normalize channel steepness indexes, we used a reference concavity (θ_{ref}) of 0.5, because in
32
33 264 practice, it is found that values of θ_{ref} between 0.4 and 0.5 work well for most mountain rivers
34
35
36 265 (Kirby & Whipple, 2012). Normalization of the channel steepness index allows for the
37
38 266 comparison of river profile morphology between streams and watersheds of different drainage
39
40
41 267 areas.

42
43
44 268

45 46 47 269 **3.b.2. Catchment-averaged local relief**

48
49 270 Local relief is the difference between minimum and maximum elevations within a specified
50
51
52 271 distance and is strongly correlated with erosion rate (Ahnert, 1970; Montgomery & Brandon,
53
54
55
56
57
58
59
60

1
2
3 272 2002; Kirby *et al.* 2003; Dibiase *et al.* 2010), which is well-correlated to rock uplift rate (e.g.
4
5
6 273 Kirby & Whipple, 2001; Lague, 2014) We used 1km radius circle to generate local relief.
7
8
9 274

10 275 **3.c. Cosmogenic nuclide burial age dating**

11
12
13 276 The ages of the Alazani series sediments are particularly important as the age of these
14
15 277 syntectonic sediments could help constrain the age of initiation of this portion of the KFTB.
16
17 278 Because the Alazani series sediments lack abundant ash horizons and are mostly too coarse
18
19 279 grained for magnetostratigraphy or the preservation of microfauna useful for biostratigraphic
20
21 280 correlation, we attempted to constrain the age of these sediments through the use of
22
23 281 cosmogenic nuclide burial age dating. Terrestrial cosmogenic nuclides (TCNs), such as ^{10}Be and
24
25 282 ^{26}Al , are produced by the interaction of secondary particles, produced in the Earth's
26
27 283 atmosphere during interaction with cosmic rays, with Earth materials (e.g. see review by Gosse
28
29 284 & Philips, 2001). The accumulation of TCN in Earth materials is a function of depth, the duration
30
31 285 of exposure, the erosion rate of the surface, and the production rate of the isotope in question,
32
33 286 which is a function of latitude and elevation. Importantly, production of TCNs goes to zero
34
35 287 below an attenuation depth such that virtually all production occurs in the first 1-3 meters of
36
37 288 the Earth's surface. Measuring the cosmogenic nuclide abundances in sediment eroded from
38
39 289 upland catchments and then deposited in adjacent basins records both a paleo erosion rate and
40
41 290 a time since burial (e.g. Granger *et al.* 1997; Granger & Muzikar, 2001; Granger, 2006). As there
42
43 291 are two unknowns, it is necessary to measure the concentration of two separate TCNs with
44
45 292 different half lives, which in this study are ^{10}Be and ^{26}Al . It is assumed that both burial of these
46
47 293 sediments and shielding from any further production of TCN post-burial (i.e. burial below
48
49
50
51
52
53
54
55
56
57
58
59
60

1
2
3 294 several meters) occurs rapidly and that the sediments in question remain shielded until nearly
4
5
6 295 the time of collection (e.g. see review by Granger, 1997).
7
8

9 296

10 297 **3.c.1. Sample collection and preparation**

11
12
13 298 Three samples were collected for cosmogenic nuclide burial age dating – GOMSS01, GOMSS02
14
15 299 and GOMSS03 (see **Error! Reference source not found.**)
16
17

18 300 *GOMSS01*

19
20
21
22 301 The site is located in the Gombori range, 1.5 km southeast from the highest peak of the range
23
24 302 called Tsivi (1991m). The sample was collected from the bottom of 1.0m deep pit. The upper
25
26 303 0.2 of this pit was soil and the rest was conglomerate of probably Al₁.
27
28

29 304 *GOMSS02*

30
31
32
33 305 The sample was taken from the lowest edge of an outcrop exposed along the Turdo river
34
35 306 (catchment 6) from probably Al₃. The sampling spot was already carved out by erosion for
36
37 307 about 1.5 – 2.0 meters, additionally we excavated back an additional 0.4 meters. Sample
38
39 308 GOMSS02 was taken from 0.5m above the floodplain and 14m below the surface of the canyon
40
41
42 309 wall. Horizontal dug depth: 0.4m, dip: 5°, dip direction: 2°.
43
44

45 310 *GOMSS03*

46
47
48
49 311 The sample was taken 500m upstream from GOMSS02 within the same outcrop belt along the
50
51 312 Turdo River, from 1.88m above the floodplain from probably Al₃. The outcrop was horizontally
52
53 313 carved by recent erosion inward ~0.9m and we excavated an additional 0.4m into the vertical
54
55
56
57
58
59
60

1
2
3 314 face. The sampling location was 66m below the surface of the canyon wall. Dip: 10⁰, dip
4
5 315 direction: 5⁰, depth from the top of the outcrop: 66m.
6
7

8
9 316 *Table 1: Burial age sampling site information*
10

11
12 317 Of the three samples collected, two (GOMSS01 and GOMSS03) yielded sufficient quartz for
13
14 318 dating. The isolation and purification of quartz, dissolution, column chemistry, and precipitation
15
16 319 of Be and Al oxides was performed in the cosmogenic isotope laboratory at Arizona State
17
18 320 University. Isolation of quartz in these samples required modification of standard methods (e.g.
19
20 321 Kohl & Nishiizumi, 1992), because of significant fractions of fine-grained, quartz rich lithic
21
22 322 material that dissolved at similar rates in HF and HNO₃ leaches as the quartz being targeted for
23
24 323 analysis. Thus, after the initial step of cleaning in Aqua Regia, instead of proceeding directly to
25
26 324 leaching in HF and HNO₃, we first used the hot phosphoric acid method (Mifsud *et al.* 2013) to
27
28 325 remove feldspars and break up these lithic clasts. After HPA, samples were leached with HF and
29
30 326 HNO₃ as in the standard procedure. After cleaning and during dissolution, samples were spiked
31
32 327 with commercial ¹⁰Be carrier. We then extracted ¹⁰Be and ²⁶Al through column chromatography
33
34 328 (Ditchburn & Whitehead, 1994) and nuclide ratios were measured via accelerator mass
35
36 329 spectrometry at the Purdue Rare Isotope (PRIME) Laboratory at Purdue University. We
37
38 330 measured native Al concentrations for the two samples using a Thermo iCAP6300 ICP-OES at
39
40 331 Arizona State University's Goldwater Environmental Laboratory.
41
42
43
44
45
46
47
48

49 332
50
51
52
53
54
55
56
57
58
59
60

333 **3.c.2. Modeling burial age dates**

334 For the two burial age samples that yielded sufficient quartz, we used CosmoCalc v3.0, a
335 Microsoft Excel add-in for cosmogenic nuclide calculations (Vermeesch, 2007). We used the
336 default settings for calibration sites for ^{10}Be and ^{26}Al production and production mechanisms
337 within CosmoCalc v3.0 and report the results of using the Burial-Exposure function within
338 CosmoCalc's Age/Erosion rate calculator, though we also tested the Burial-Erosion function,
339 which produced similar estimations of burial age. CosmoCalc provides two different numerical
340 methods for fitting burial dates, the Metropolis and Newton's method. We tested both
341 methods and found that the Metropolis method, which is more complicated, produced variable
342 burial ages, i.e. running the calculation multiple times yielded different results, but that given
343 the magnitude of the uncertainty, this variability in burial ages was small and the error ranges
344 for the simpler Newton's method were extremely large. Importantly, for most runs, the
345 reported burial age using Newton's and the Metropolis method were similar and the error
346 ranges reported from the Metropolis method were largely consistent between runs. We
347 elected to report values from the Metropolis method as these likely reflect a more reasonable
348 range of uncertainties on the burial ages (e.g. Vermeesch, 2007). To account for the variability
349 in reported burial age from multiple runs of the Metropolis method, we report the average of
350 the result of ten runs.

351 To determine a burial age, a production scaling factor must be assumed for the area that
352 originally contributed the sediment that was eventually eroded, transported, deposited and
353 then buried. While the exact parameters included in different scaling schemes vary, in general
354 latitude and elevation will be the most important factors controlling the production rate (e.g.

1
2
3 355 Gosse & Philips, 2001). Because the source of sediment for the Alazani series sediments is not
4
5
6 356 well constrained, we tested four different scaling schemes assuming different source areas.
7
8 357 Specifically, we tested a 'local' sourcing using a latitude and mean elevation appropriate for a
9
10 358 representative catchment in the northern Gombori range, and then three different sources
11
12
13 359 from the GC with representative latitudes and mean elevations for a river draining the higher
14
15 360 portions of the central GC (e.g. the modern Aragvi river), one draining an intermediate set of
16
17 361 elevations (e.g. the modern Iori river), and one draining lower elevations coming directly from
18
19
20 362 the small catchments that drain into the Alazani valley from the central and eastern GC. For
21
22
23 363 calculation of scaling factors, we use the CosmoCalc implementation of the Desilets *et al.* (2006)
24
25 364 scheme. The calculated burial ages are reported in **Error! Reference source not found.** for
26
27 365 GOMSS03, calculations were not performed for GOMSS01 as an age is not interpretable for this
28
29
30 366 sample as it plots in the region above the constant exposure line, outside the range of
31
32
33 367 physically possible results.
34
35
36 368

37 369 **4. Results**

40 370 **4.a. Paleocurrent analyses**

41
42
43 371 Paleocurrent analyses of outcrops of Al₁ in two catchments indicate that Al₁ sediments were
44
45 372 deposited by a river flowing in a SW direction through the modern Gombori Range, counter to
46
47
48 373 the modern drainage direction and consistent with rivers sourced from the Greater Caucasus.
49
50 374 The same analyses in the younger, stratigraphically higher Al₃, paleocurrents no longer indicate
51
52
53 375 a single, dominant flow direction but are generally consistent with dominantly southward or
54
55 376 eastward flow (see Figure 7 and
56
57
58
59
60

1
2
3 3774
5
6 378 Table 2. *Von Mises distribution results for the paleocurrent measurements*7
8
9 37910
11
12 380).13
14
15 38116
17
18 382 Table 2. *Von Mises distribution results for the paleocurrent measurements*19
20
21 38322
23
24
25 384 **4.b. Tectonic geomorphology**

26
27 385 Quantitative tectonic geomorphologic analyzes show higher channel steepness indexes from
28
29 386 the western catchments. Catchment-averaged local relief is also higher in the western
30
31 387 catchments (Figure 8), which is consistent with the observation in many landscapes that mean
32
33 388 normalized channel steepness and local relief are often linearly related (Dibiase *et al.* 2010). A
34
35 389 simple interpretation of these two indices would suggest that the western part of Gombori
36
37 390 range is uplifting faster than its eastern segment.

38
39
40
41
42 391 As noted above, tectonic geomorphologic proxies could be influenced by rainfall and lithology.

43
44
45 392 Indeed there are strong correlations between rainfall and each of catchment-mean elevation,
46
47 393 local relief and mean K_{sn} ($r^2=0.84$, $r^2=0.68$ and $r^2=0.89$, respectively) This likely reflects expected
48
49 394 orographic enhancement of rainfall such that areas of high relief, channel steepness and mean
50
51 395 elevation driven by high rock-uplift rates are associated with high rates of precipitation.

52
53
54 396 Importantly, a climatic control on topography would imply reduced relief and channel

55
56
57
58
59
60

1
2
3 397 steepness in areas of enhanced precipitation. Thus, interpreting topography as reflecting rock
4
5
6 398 uplift rate patterns alone is a conservative assumption. We also checked whether lithology
7
8 399 importantly influenced our tectonic geomorphologic indexes, but correlations between
9
10
11 400 dominant rock types and geomorphologic proxies are low (Figure 9), as the correlation
12
13 401 coefficients between mean K_{sn} and K (Cretaceous rocks) and Ak-Ap (Akchagyl-Apsheron
14
15 402 sediments) are 0.42 and -0.46. Higher slopes of conglomerate dominated catchments could be
16
17
18 403 explained by the tendency of the conglomerate deposits to be exposed as cliffs.

19
20
21 404 The correlation matrix in Figure 9 shows very high correlation between mean K_{sn} and elevation
22
23 405 (0.95), implying faster uplift rates in the center of the Gombori range, an assumption generally
24
25
26 406 consistent with the deeper levels of exposure in the center of the range, i.e. Cretaceous rocks
27
28 407 (Figure 7 & Figure 10).

31 408 **4.c. Burial age dates**

32
33
34 409 **Error! Reference source not found.** summarizes the analytical results. Unfortunately, one of
35
36 410 our samples, GOMSS01, yielded a $^{26}\text{Al}/^{10}\text{Be}$ ratio that even within the uncertainty bounds plots
37
38
39 411 entirely above the constant exposure line of the standard erosion island plot, in the so-called
40
41 412 'forbidden zone' (Figure 11). Data that plots in this region is physically impossible as the
42
43
44 413 $^{26}\text{Al}/^{10}\text{Be}$ ratio cannot exceed the ratio of the production rates of the two isotopes because ^{26}Al
45
46 414 decays faster than ^{10}Be . This suggests that there was a methodological error during processing,
47
48
49 415 thus a burial age is not interpretable from this sample. The other sample, GOMSS03, did yield
50
51 416 an interpretable age, but because of relatively high concentrations of native Al and low
52
53
54 417 concentrations of ^{26}Al , the analytical precision of this measurement is quite low, yielding a
55
56 418 burial age of ~ 1.0 Ma, with lower and upper bounds of 0.005 Ma and 2.5 Ma, respectively (see
57
58
59
60

1
2
3 419 **Error! Reference source not found.** for complete results). While imprecise, given that there are
4
5
6 420 no published geochronologic ages for the age of the Alazani series, or more broadly for any of
7
8 421 the sediments in this region of the KFTB, this age is still meaningful as it confirms that these
9
10 422 sediments are most likely Apsheronian in age. Because of the relatively low ^{10}Be concentration
11
12 423 and thus the relatively high implied paleo-erosion rates, the uncertainty in source area for the
13
14 424 sediment and associated uncertainty in applicable production scheme does not significantly
15
16 425 influence the interpreted age for sample GOMSS03, but does have implications for the implied
17
18 426 paleo erosion rate (Figure 11). The minimum and maximum scaling for sample GOMSS03 would
19
20 427 imply paleo erosion rates within the source area of between ~ 20 cm/ka to ~ 35 cm/ka,
21
22 428 respectively.
23
24
25
26
27
28
29
30
31

32 430 **5. Discussion**

33 34 431 **5.a. Initiation and development of the western Kura Fold Thrust Belt**

35
36
37 432 The results of our paleocurrent analyses suggest that a major drainage reorganization and flow
38
39 433 reversal of rivers within the western KFTB started during or after the deposition of the Al_1 facies
40
41 434 within the Alazani Series and finished during or after deposition of the Al_3 facies. We attribute
42
43 435 this drainage reorganization to formation, or intensification of uplift, of the western KFTB at
44
45 436 this longitude during the time period spanning the deposition of the Alazani Series (Figure 12).
46
47
48
49

50 437 Our field measurements show that Al_1 facies have higher dip angles (50° - 60°), Al_2 has moderate
51
52 438 – 20° - 30° dip angles, and the youngest Al_3 facies have the shallowest dips – 5° - 15° (e.g. Figure
53
54 439 7), broadly suggestive that these strata are syn-tectonic, i.e. they are growth strata. The
55
56
57
58
59
60

1
2
3 440 sediments of the Alazani series were previously mapped as being a part of the Akchagyl-
4
5
6 441 Apsheron stages. The reported age for the base of the Akchagyl is variable between publications
7
8 442 and regions (e.g. Krijgsman *et al.* 2019), but it has been constrained to be ~2.7 Ma near the
9
10 443 Azerbaijan Caspian Sea coast based on $^{40}\text{Ar}/^{39}\text{Ar}$ dating of an ash horizon (Van Baak *et al.*
11
12 444 2019b). It is suggested that the base of the Akchagyl may be time transgressive and in a section
13
14
15 445 ~150 km to the east of the Gombori range it has been constrained to be ~2.5 Ma based on the
16
17
18 446 maximum depositional age from detrital zircons in the strata below the Akchagyl (Forte *et al.*
19
20 447 2015). The boundary between the Akchagyl and Apsheron stages are similarly variable, but in
21
22 448 the vicinity of the KFTB, the Apsheron has been dated to extend from 2.2 to 0.88 Ma (e.g.
23
24
25 449 Krijgsman *et al.* 2019).

26
27
28 450 According to this information, we make an attempt to estimate the ages and reconstruct the
29
30
31 451 depositional environment and tectonic context of the Alazani series. Deposition of Al_1
32
33 452 sediments started not earlier than ca. 2.7-2.5 Ma years ago by the streams flowing from the GC
34
35
36 453 to the southwest through the location of the modern Gombori range area into the Kura basin.
37
38 454 We hypothesize that during deposition of Al_1 , uplift of the Gombori range initiated, and
39
40
41 455 potentially damming the formerly south flowing rivers, which could explain the finer, more
42
43 456 lacustrine sediments in Al_2 , though given the uncertainty in the exact age of the Al_2 facies and
44
45
46 457 the broad context of the Akchagyl stage as a transgressive event, it is not possible to rule out a
47
48 458 more regional explanation for the lacustrine character of the Al_2 facies. Regardless, by the time
49
50 459 of deposition of Al_3 , sufficient deformation and uplift had accrued in the Gombori range to
51
52
53 460 effect a significant drainage reorganization and the development of (1) a set of north flowing
54
55 461 rivers on the Gombori range and (2) an axial valley, i.e. the Alazani valley, between the Gombori
56
57
58
59
60

1
2
3 462 and the GC. We interpret the lack of a dominant paleocurrent direction in these Al₃ facies
4
5
6 463 sediments to reflect possible deposition within this axial valley, which today is dominated by a
7
8 464 set of meandering fluvial systems. This would imply that the northwestern extent of the
9
10
11 465 Gombori range has expanded since the deposition of Al₃, i.e. at the time of deposition the
12
13 466 paleocurrent sites were not within the deformed part of the Gombori range, but have
14
15 467 subsequently be incorporated into the range. Comparison between the interpreted paleo-
16
17
18 468 drainage network and the modern drainage network, suggests that uplift in the Gombori range
19
20 469 was sufficiently rapid such that river(s) could not maintain antecedent gorges like they currently
21
22
23 470 do in the eastern KFTB (see Forte *et al.* 2010).

24
25
26 471 The lack of precise age control for the Alazani series sediments and that our one successful
27
28 472 burial age date only provides constraint for the time by which a drainage reorganization had
29
30
31 473 been completed results in uncertainty in terms of when deformation initiated in the western
32
33 474 KFTB. However, if we assume that (1) the age of the base of the Al₁ strata is between 2.7-2.5
34
35 475 Ma (the maximum permissible age of the Akchagyl stage in this region), and (2) reflects
36
37
38 476 deposition before significant development of the western KFTB and that the age of the Al₃
39
40
41 477 strata is ~1 Ma (from our burial age date of sample GOMSS03), and (3) deposition of Al₃ reflects
42
43 478 a time by which the drainage reorganization had been completed, this brackets the initiation
44
45 479 age of the western KFTB to between 2.7 and 1 Ma. Comparison of this range of possible
46
47
48 480 initiation ages with those observed in the far eastern end of the KFTB, which based on new age
49
50 481 constraints (e.g. Lazarev *et al.* 2019) likely initiated at ~2.2-2.0 Ma, suggests that if there was
51
52
53 482 eastward along-strike propagation of the KFTB as suggested by Forte *et al.* (2010), it took no
54
55 483 more than 0.5-1 Ma. Given the lingering uncertainty in the initiation age of the western KFTB
56
57
58
59
60

1
2
3 484 and the newly revised, older age of initiation in the eastern KFTB, it is equally viable that there
4
5 485 was no significant propagation along-strike. This uncertainty highlights the need for additional
6
7 486 work to establish the ages of the Alazani series stratigraphy in the western KFTB and identify
8
9
10 487 additional areas where the timing of initiation of the KFTB can be assessed along strike.
11
12
13
14 488

16 489 **5.b. Implications for regional tectonics and seismic hazard**

17
18
19 490 Coarse spatial resolution GPS-derived crustal motion velocity data suggests an eastward horizontal
20
21 491 velocity increase along-strike within the KFTB (see Reilinger *et al.* 2006). However, our tectonic
22
23 492 geomorphologic analyses suggest that the rates of uplift along-strike within the Gombori range are not
24
25 493 well-correlated with GPS horizontal velocities (with respect to Eurasia). In detail, our results indicate that
26
27 494 the western Gombori range may be experiencing more rapid uplift, leading to its generally higher
28
29 495 elevation, normalized channel steepness, and local relief. There could be several explanations for this
30
31 496 apparent disconnect between an eastward increase in GPS velocity with an eastward decrease in local
32
33 497 relief within the Gombori: 1) the along-strike decrease in relief reflects structural complexity with larger
34
35 498 portions of the total convergence being taken up by additional structures to the south east of the
36
37 499 Gombori, 2) an along-strike change in the ratio of shortening accommodated either currently or through
38
39 500 time between the KFTB and the interior of the GC, 3) an along-strike change in structural geometry
40
41 501 between steeper to shallower dipping structures from west to east within the KFTB that would result in
42
43 502 an eastward decrease in the relationship between incremental total-shortening and vertical rock uplift,
44
45 503 4) a first order control from lithology such that once there is sufficient exhumation to expose older,
46
47 504 more resistant units in the core of folds this lead to an increase in relief compared to adjacent areas
48
49 505 which expose younger, less resistant units, even if those areas are experiencing greater rates of rock
50
51 506 uplift, 5) the modern GPS velocity field is not representative of the long-term, i.e. several million year,
52
53
54
55
56
57
58
59
60

1
2
3 507 rate of convergence in the region, a suggestion which has been made more broadly for the GC as a
4
5 508 whole (Forte *et al.* 2016), or 6) the Gombori itself reflects an eastward propagating set of structures.

7
8 509 At present, we do not have the data to uniquely select between these hypotheses. Option 1 would be
9
10 510 consistent with coarse resolution syntheses of structures and estimation of activity of those structures
11
12 511 presented in Forte *et al.* (2010), but without quantitative assessments of the amounts of total
13
14 512 shortening accommodated by structures southeast of the Gombori (or in the Gombori itself), this is hard
15
16 513 to validate. Similarly, option 2 would be consistent with an eastward along-strike decrease in range front
17
18 514 sinuosity for the frontal GC, used as a proxy for time since the GC range front fault was active at the
19
20 515 surface, as noted by Forte *et al.*, 2010, but generally not consistent with other observations within the
21
22 516 Eastern GC of no clear differences along-strike in terms of the tectonic geomorphology of this portion of
23
24 517 the range (e.g. Forte *et al.* 2014, Forte *et al.* 2015). Option 3 is not broadly consistent with the observed
25
26 518 bedding orientations within the Gombori as, at least within the Alazani Series, there does not appear to
27
28 519 be any clear change in the orientation of units along-strike, e.g. Al₁ facies sediments uniformly dip 50°-
29
30 520 60° along the exposed portion of the Alazani series. For option 4, our analyses of the topography did not
31
32 521 indicate that lithology exerts a strong control, but importantly our analyzes did not extend beyond the
33
34 522 Gombori range. Fully evaluating option 5 or 6 requires detailed estimations of total-shortening and
35
36 523 timing of initiation along-strike within the KFTB and the Gombori, however it is worth noting that as
37
38 524 discussed in the previous section, our results along with updated chronology for stage boundaries, have
39
40 525 narrowed the range of time over which the KFTB would need to propagate eastward along-strike,
41
42 526 leaving open the possibility that a fundamental disconnect between GPS rates and long-term geologic
43
44 527 rates is viable. Ultimately, this work further highlights the necessity of detailed estimates of amounts of
45
46 528 total shortening and ages of deformation initiation throughout the KFTB.

47
48
49
50
51
52
53
54 529 Previous work from the Eastern (Forte *et al.* 2013) and Central (Alania *et al.* 2017) KFTB concluded that
55
56 530 Kura foreland is an active fold-thrust belt. Our study revealed that the Western portion of this belt has
57
58
59
60

1
2
3 531 experienced large scale tectonic movements and drainage reorganization that are still in progress. GPS
4
5 532 data from the western neighboring region showed that Tbilisi and the northern boundary of the Lesser
6
7 533 Caucasus is a zone of active convergence (Sokhadze *et al.* 2018) and the sparse GPS network from the
8
9 534 Gombori range and GC indicated horizontal velocity gradient between the Gombori and the GC (after
10
11 535 Akhalaia, Onur *et al.* 2019). All these data, from different sources lead us to assume that the Western
12
13
14 536 KFTB is actively deforming and it should be considered during seismic hazard assessment of the region.
15
16
17 537

20 538 **6. Conclusions**

21
22 539 Our synthesis of the tectonic geomorphology, absolute age dating of syn-tectonic Plio-
23
24 540 Pleistocene sediments within the Kura Fold-Thrust Belt, and paleocurrent analyses within those
25
26 541 same sediments shed new light on both the history and current state of active deformation
27
28 542 within the Western Kura Fold-Thrust Belt. The results reveal a Plio-Pleistocene drainage
29
30 543 reorganization event within the northwestern corner of the southeastern foreland of the
31
32 544 Greater Caucasus Mountains, which appears linked to initiation and development of the Kura
33
34 545 Fold-Thrust Belt. If the timing of this drainage reorganization event, constrained to have
35
36 546 occurred between ~2.7-1 Ma, is representative of initiation of this western-most segment of
37
38 547 the KFTB, then this is still consistent with the idea of an eastward propagating KFTB as originally
39
40 548 proposed by Forte *et al.* (2010), but implies that along-strike propagation of the fold-thrust belt
41
42 549 along its ~300 km length took no more than ~1 million years and leaves open the possibility of
43
44 550 no significant along-strike diachroneity in fold-thrust belt initiation. Quantitative tectonic
45
46 551 geomorphic analyses of the Gombori range indicate that the Western Kura Fold-Thrust belt is
47
48 552 still a zone of active deformation, especially its NW segment. This is consistent with recently
49
50
51
52
53
54
55
56
57
58
59
60

1
2
3 553 published, preliminary GPS velocity data (after Akhalaia, Onur *et. al*, 2019) suggestive of a
4
5
6 554 velocity gradient between the Western Kura Fold-Thrust Belt and Greater Caucasus Mountains.
7
8 555 In aggregate, our results highlight that potential seismic activity within the Gombori Range and
9
10 556 northwestern Kura Fold-Thrust Belt should be considered when assessing seismic hazard for the
11
12
13 557 densely populated (~1.2 million people) Georgian capital city of Tbilisi, which lies less than 50
14
15 558 km away from our study sites.
16
17

18 559

20
21
22 560 *Supplementary Material is available on the Cambridge Journals Online website*
23
24
25
26
27
28
29
30
31
32
33
34
35
36
37
38
39
40
41
42
43
44
45
46
47
48
49
50
51
52
53
54
55
56
57
58
59
60

1
2
3 562 **Acknowledgments**
4
5

6 563 This work was supported by:
7
8

9 564 This research [#PhDF2016_208 and #IG 29/1/16] has been supported by Shota Rustaveli
10
11

12 565 National Science Foundation of Georgia (SRNSFG);
13
14

15 566 Louisiana State University;
16
17

18 567 United States National Science Foundation grant EAR-1450970 to Adam M. Forte and Kelin X.
19
20

21 568 Whipple;
22
23

24 569 Institute of Earth Sciences and National Seismic Monitoring Centre, Ilia State University;
25
26

27 570 Arizona State University.
28
29

30 571
31

32 572 **Conflict of interest.** None
33
34
35
36
37
38
39
40
41
42
43
44
45
46
47
48
49
50
51
52
53
54
55
56
57
58
59
60

1
2
3 574 *Figure 1. Location and topography of KFTB*
4
5

6 575 Figure 2. Earthquake events of KFTB from Complete Catalogue of Instrumental Seismicity for
7
8
9 576 Georgia (Onur *et al.* 2019), fault plane solution by (Tan & Taymaz, 2006)
10

11
12 577 Figure 3. Stratigraphy of the Gombori range compiled after (Buleishvili, 1974), (Zedginidze *et al.*
13
14 578 1971), (Kereselidze, 1950), (Sidorenko & Gamkrelidze, 1964), (Buachidze *et al.* 1950).
15

16
17 579 Thicknesses are approximate and likely vary along-strike within the Gombori Range
18

19
20 580 Figure 4. Base of Al1 series from catchment 7, view to the NW showing steeply, NE dipping
21
22 581 conglomeratic (a) and sandy loam (b) beds
23
24

25
26 582 Figure 5. NE dipping volcanic ash layer exposed in catchment 12, facies 2
27

28
29 583 Figure 6. TRMM 3B42 pixel extends (black) and catchments of the study area (red) and the
30
31 584 identifying numbers for those catchments referenced in the text
32
33

34
35 585 Figure 7. Simplified lithology, sampling sites and paleocurrent directions
36
37

38 586 Figure 8. Topography and local relief maps of catchments (upper). Catchment averaged and
39
40 587 stream k_{sn} values (below). See text for details of these calculations
41
42

43
44 588 Figure 9. correlation matrix of different indices. Units: Local relief – meter; Mean elevation –
45
46 589 meter; Mean slope – degree; K (Cretaceous rocks) – Percentage of catchment covered by these
47
48 590 rocks; AkAp (Akchagyl-Apsheron) - Percentage of catchment covered by these rocks; TRMM -
49
50 591 millimeter/annual mean
51
52
53
54
55
56
57
58
59
60

1
2
3 592 Figure 10. Swath profile of topography, k_{sn} values (upper graph) and along swath
4
5
6 593 geomorphologic indices and rainfall data
7
8

9 594 Figure 11. Erosion island plot for Gombori range samples. Variability in production rate scaling
10
11 595 for the two samples, GOMSS01 and GOMSS03 are reflected in the pairs of points. Sample
12
13 596 GOMSS01 plots in the forbidden zone and are thus interpretable. Sample GOMSS03 have mean
14
15
16 597 ages of ~ 1 Ma regardless of exact scaling relationships used. The relatively high uncertainties on
17
18 598 the ages reflect high native Al concentrations. Burial isochrons are reported in Ma and bounds
19
20
21 599 for estimated paleo erosion rates in cm/ka. Plots produced using CosmoCalc (Vermeesch, 2007)
22
23

24 600 Figure 12. Fluvial system evolution diagram for the western KFTB. A) During the deposition of
25
26 601 Alazani Suite1 (Al_1), rivers draining from the Greater Caucasus were still able to flow directly
27
28 602 south across what is now the KFTB. B) Alazani Suite 2 (Al_2) represents deposition in a lacustrine
29
30
31 603 setting, which could relate to damming of rivers by growth of the KFTB, or could be related to
32
33 604 broader, basin wide changes in base-level. C) By the time of deposition of Alazani Suite 3 (Al_3),
34
35
36 605 the river network in the northwestern KFTB had developed into something similar to the
37
38 606 modern, with rivers draining northward out of the Gombori range and with a well-defined axial
39
40
41 607 drainage occupying the Alazani basin
42
43
44
45
46
47
48
49
50
51
52
53
54
55
56
57
58
59
60

609 *Table 1. Burial age sampling site information*

Sample name	Date of collection	Location	Elevation (m)	Facies
GOMSS01	26-Apr-2017	41.80815, 45.34789	1831	Al ₁ (?)
GOMSS02	09-Mar-2017	41.92953, 45.40144	749	Al ₃
GOMSS03	09-Mar-2017	41.928925, 45.395784	768	Al ₃

Proof For Review

611 Table 2. Von Mises distribution results for the paleocurrent measurements

Catchment	Facies	Number of measurements	Max value (%)	Orientation (deg.)	Mean vector (deg.)
7	Al ₁	36	56	221-240	225.4±3.6
7	Al ₃	52	17	61-80	142.4±20.4
11	Al ₁	93	63	201-220	214.7±2.2
11	Al ₃	73	18	101-120	67±25.8

613 **References**

- 614 Adamia, Sh, V. Alania, A. Chabukiani, G. Chichua, O. E nukidze, & N. Sadradze. 2010. "Evolution
615 of the Late Cenozoic Basins of Georgia (SW Caucasus): A Review." *Geological Society Special
616 Publication* 340: 239–59. <https://doi.org/10.1144/SP340.11>.
- 617 Adamia, Shota, Victor Alania, Aleksandre Chabukiani, Zurab Kutelia, & Nino Sadradze. 2011.
618 "Great Caucasus (Cavcasioni): A Long-Lived North-Tethyan Back-Arc Basin" 20: 611–28.
619 <https://doi.org/10.3906/yer-1005-12>.
- 620 Ahnert, Frank. 1970. "Functional Relationships between Denudation, Relief, and Uplift in Large,
621 Mid-Latitude Drainage Basins." *American Journal of Science* 268: 243–63.
622 <https://doi.org/10.2475/ajs.268.3.243>.
- 623 Alania, Victor, A. Chabukiani, R. Chagelishvili, Onice E nukidze, K. Gogrichiani, A. Razmadze, &
624 Nino Tsereteli. 2017. "Growth Structures, Piggy-Back Basins and Growth Strata of the
625 Georgian Part of the Kura Foreland Fold-Thrust Belt: Implications for Late Alpine Kinematic
626 Evolution." *Geological Society, London, Special Publications* 428: 171–85.
627 <https://doi.org/10.1144/SP428.5>.
- 628 Allmendinger, Richard W., Nestor Cardozo, & Donald M. Fisher. 2011. *Structural Geology
629 Algorithms*. <https://doi.org/10.1017/CBO9780511920202>.
- 630 Avdeev, Boris, & Nathan A. Niemi. 2011. "Rapid Pliocene Exhumation of the Central Greater
631 Caucasus Constrained by Low-Temperature Thermochronometry." *Tectonics*.
632 <https://doi.org/10.1029/2010TC002808>.
- 633 Baak, Christiaan G.C. Van, Arjen Grothe, Keith Richards, Marius Stoica, Elmira Aliyeva, Gareth R.
634 Davies, Klaudia F. Kuiper, & Wout Krijgsman. 2019a. "Flooding of the Caspian Sea at the

- 1
2
3 635 Intensification of Northern Hemisphere Glaciations." *Global and Planetary Change* 174:
4
5
6 636 153–63. <https://doi.org/10.1016/j.gloplacha.2019.01.007>.
7
8
9 637 Bookhagen, Bodo, & Douglas W. Burbank. 2006. "Topography, Relief, and TRMM-Derived
10
11 638 Rainfall Variations along the Himalaya." *Geophysical Research Letters* 33 (8): 1–5.
12
13
14 639 <https://doi.org/10.1029/2006GL026037>.
15
16
17 640 Bookhagen, Bodo, & Manfred R. Strecker. 2008. "Orographic Barriers, High-Resolution TRMM
18
19 641 Rainfall, and Relief Variations along the Eastern Andes." *Geophysical Research Letters* 35
20
21 642 (6): 1–6. <https://doi.org/10.1029/2007GL032011>.
22
23
24
25 643 Bretis, Bernhard, Nikolaus Bartl, & Bernhard Grasemann. 2011. "Lateral Fold Growth and
26
27 644 Linkage in the Zagros Fold and Thrust Belt (Kurdistan, NE Iraq)." *Basin Research* 23 (6):
28
29 645 615–30. <https://doi.org/10.1111/j.1365-2117.2011.00506.x>.
30
31
32
33 646 Buachidze, I, K Gigauri, I Zviadadze, & T Pkhakadze. 1950. "Groundwater Resource Estimations
34
35 647 of Alazani Artesian Basin (in Russian)." Tbilisi: Ministry of Geology of USSR.
36
37
38 648 Buachidze, I, T Pkhakadze, & Sh Tsitsilashvili. 1952. "Alazani Artesian Basin (In Russian)." Tbilisi.
39
40
41
42 649 Burbank, Douglas, Andrew Meigs, & Nicholas Brozović. 1996. "Interactions of Growing Folds
43
44 650 and Coeval Depositional Systems." *Basin Research* 8 (3): 199–223.
45
46 651 <https://doi.org/10.1046/j.1365-2117.1996.00181.x>.
47
48
49
50 652 Champel, Bénédicte. 2002. "Growth and Lateral Propagation of Fault-Related Folds in the
51
52 653 Siwaliks of Western Nepal: Rates, Mechanisms, and Geomorphic Signature." *Journal of*
53
54 654 *Geophysical Research* 107 (B6). <https://doi.org/10.1029/2001jb000578>.
55
56
57
58
59
60

- 1
2
3 655 Chkhikvadze, V, G Mchedlidze, N Burchak-Abramovich, O Bendukidze, D Burchak, Ts Gabelaia, N
4
5
6 656 Amiranashvili, G Meladze, E Kharabadz, & N Chkareuli. 2000. "Review of the Localities of
7
8 657 Tertiary Vertebrates of Georgia (In Russian)." In , 153–60. Tbilisi: A. Janelidze Geological
9
10 658 Institute, Georgian Academy of Sciences.
- 11
12
13
14 659 Cowgill, Eric, Adam M. Forte, Nathan Niemi, Boris Avdeev, Alex Tye, Charles Trexler, Zurab
15
16 660 Javakhishvili, Mikheil Elashvili, & Tea Godoladze. 2016. "Relict Basin Closure and Crustal
17
18 661 Shortening Budgets during Continental Collision: An Example from Caucasus Sediment
19
20 662 Provenance." *Tectonics* 35 (12): 2918–47. <https://doi.org/10.1002/2016TC004295>.
- 21
22
23
24 663 Davis, Kenneth, Douglas W Burbank, Donald Fisher, Shamus Wallace, & David Nobes. 2005.
25
26 664 "Thrust-Fault Growth and Segment Linkage in the Active Ostler Fault Zone , New Zealand."
27
28 665 *Journal of Structural Geology* 27: 1528–46. <https://doi.org/10.1016/j.jsg.2005.04.011>.
- 29
30
31
32 666 Delcaillau, B., B. Deffontaines, L. Floissac, J. Angelier, J. Deramond, P. Souquet, H. T. Chu, & J. F.
33
34 667 Lee. 1998. "Morphotectonic Evidence from Lateral Propagation of an Active Frontal Fold;
35
36 668 Pakuashan Anticline, Foothills of Taiwan." *Geomorphology* 24 (4): 263–90.
37
38 669 [https://doi.org/10.1016/S0169-555X\(98\)00020-8](https://doi.org/10.1016/S0169-555X(98)00020-8).
- 39
40
41
42 670 Delcaillau, Bernard. 2001. "Geomorphic Response to Growing Fault-Related Folds: Example
43
44 671 from the Foothills of Central Taiwan." *Geodinamica Acta* 14 (5): 265–87.
45
46 672 <https://doi.org/10.1080/09853111.2001.11432447>.
- 47
48
49
50 673 Delcaillau, Bernard, Jean Michel Carozza, & Edgard Laville. 2006. "Recent Fold Growth and
51
52 674 Drainage Development: The Janauri and Chandigarh Anticlines in the Siwalik Foothills,
53
54 675 Northwest India." *Geomorphology* 76 (3–4): 241–56.
- 55
56
57
58
59
60

- 1
2
3 676 <https://doi.org/10.1016/j.geomorph.2005.11.005>.
4
5
6 677 Desilets, Darin, Marek Zreda, & T. Prabu. 2006. "Extended Scaling Factors for in Situ
7
8 678 Cosmogenic Nuclides: New Measurements at Low Latitude." *Earth and Planetary Science*
9
10 679 *Letters* 246 (3–4): 265–76. <https://doi.org/10.1016/j.epsl.2006.03.051>.
11
12
13
14 680 Dibiase, Roman A, Kelin X Whipple, Arjun M Heimsath, & William B Ouimet. 2010. "Landscape
15
16 681 Form and Millennial Erosion Rates in the San Gabriel Mountains , CA." *Earth and Planetary*
17
18 682 *Science Letters* 289 (1–2): 134–44. <https://doi.org/10.1016/j.epsl.2009.10.036>.
19
20
21
22 683 Ditchburn, & Whitehead. 1994. "The Separation of ^{10}Be from Silicates." *3rd Workshop of the*
23
24 684 *South Pacific Environmental Radioactivity Association*.
25
26
27
28 685 Douglass, John, & Mark Schmeuckle. 2007. "Analogue Modeling of Transverse Drainage
29
30 686 Mechanisms." *Geomorphology* 84 (1–2): 22–43.
31
32 687 <https://doi.org/10.1016/j.geomorph.2006.06.004>.
33
34
35
36 688 Flint, J. J. 1974. "Stream Gradient as a Function of Order, Magnitude, and Discharge." *Water*
37
38 689 *Resources Research* 10 (5): 969–73. <https://doi.org/10.1029/WR010i005p00969>.
39
40
41 690 Forte, A. M., E. Cowgill, T. Bernardin, O. Kreylos, & B. Hamann. 2010. "Late Cenozoic
42
43 691 Deformation of the Kura Fold-Thrust Belt, Southern Greater Caucasus." *Bulletin of the*
44
45 692 *Geological Society of America* 122 (3–4): 465–86. <https://doi.org/10.1130/B26464.1>.
46
47
48
49 693 Forte, A. M., & Eric Cowgill. 2013. "Late Cenozoic Base-Level Variations of the Caspian Sea: A
50
51 694 Review of Its History and Proposed Driving Mechanisms." *Palaeogeography,*
52
53 695 *Palaeoclimatology, Palaeoecology* 386: 392–407.
54
55
56
57
58
59
60

- 1
2
3 696 <https://doi.org/10.1016/j.palaeo.2013.05.035>.
4
5
6 697 Forte, A. M., Eric Cowgill, Ibrahim Murtuzayev, Talat Kangarli, & Marius Stoica. 2013. "Structural
7
8 698 Geometries and Magnitude of Shortening in the Eastern Kura Fold-Thrust Belt, Azerbaijan:
9
10 699 Implications for the Development of the Greater Caucasus Mountains." *Tectonics* 32 (3):
11
12 700 688–717. <https://doi.org/10.1002/tect.20032>.
13
14
15
16 701 Forte, A. M., Eric Cowgill, & Kelin X. Whipple. 2014. "Transition from a Singly Vergent to Doubly
17
18 702 Vergent Wedge in a Young Orogen: The Greater Caucasus." *Tectonics* 33 (11): 2077–2101.
19
20 703 <https://doi.org/10.1002/2014TC003651>.
21
22
23
24 704 Forte, A. M., Dawn Y. Sumner, Eric Cowgill, Marius Stoica, Ibrahim Murtuzayev, Talat Kangarli,
25
26 705 Mikheil Elashvili, Tea Godoladze, & Zurab Javakhishvili. 2015. "Late Miocene to Pliocene
27
28 706 Stratigraphy of the Kura Basin, a Subbasin of the South Caspian Basin: Implications for the
29
30 707 Diachroneity of Stage Boundaries." *Basin Research* 27 (3): 247–71.
31
32 708 <https://doi.org/10.1111/bre.12069>.
33
34
35
36
37 709 Forte, A. M., Kelin X. Whipple, & Eric Cowgill. 2015. "Drainage Network Reveals Patterns and
38
39 710 History of Active Deformation in the Eastern Greater Caucasus." *Geosphere* 11 (5): 1343–
40
41 711 64. <https://doi.org/10.1130/GES01121.1>.
42
43
44
45 712 Forte, A. M., & Kelin X Whipple. 2018. "Short Communication : The Topographic Analysis Kit
46
47 713 (TAK) for TopoToolbox." *Earth Surface Dynamics*, no. July: 1–9.
48
49 714 <https://doi.org/10.5194/esurf-2018-57>.
50
51
52
53 715 Forte, A. M, Kelin X Whipple, Bodo Bookhagen, & Matthew W Rossi. 2016. "Decoupling of
54
55
56
57
58
59
60

- 1
2
3 716 Modern Shortening Rates , Climate , and Topography in the Caucasus.” *Earth and*
4
5
6 717 *Planetary Science Letters* 449: 282–94. <https://doi.org/10.1016/j.epsl.2016.06.013>.
7
8
9 718 Gallen, Sean F., & Karl W. Wegmann. 2017. “River Profile Response to Normal Fault Growth and
10
11 719 Linkage: An Example from the Hellenic Forearc of South-Central Crete, Greece.” *Earth*
12
13 720 *Surface Dynamics* 5 (1): 161–86. <https://doi.org/10.5194/esurf-5-161-2017>.
14
15
16
17 721 Gosse, & Philips. 2001. “Terrestrial in Situ Cosmogenic Nuclides:Theory and Application.”
18
19 722 *Quaternary Science Reviews* 20: 1475–1560.
20
21
22 723 Granger, Darryl E., James W.Kirchner, & Robert C. Finkel. 1997. “Quaternary Downcutting Rate
23
24 724 of the New River, Virginia, Measured from ^{26}Al and ^{10}Be in Cave-Deposited Alluvium.”
25
26 725 *Geology* 25 (2): 107–10. [https://doi.org/10.1130/0091-](https://doi.org/10.1130/0091-7613(1997)025<0107:QDROTN>2.3.CO;2)
27
28
29 726 [7613\(1997\)025<0107:QDROTN>2.3.CO;2](https://doi.org/10.1130/0091-7613(1997)025<0107:QDROTN>2.3.CO;2).
30
31
32
33 727 Granger, Darryl E., & Paul F. Muzikar. 2001. “Dating Sediment Burial with in Situ-Produced
34
35 728 Cosmogenic Nuclides: Theory, Techniques, and Limitations.” *Earth and Planetary Science*
36
37 729 *Letters* 188 (1–2): 269–81. [https://doi.org/10.1016/S0012-821X\(01\)00309-0](https://doi.org/10.1016/S0012-821X(01)00309-0).
38
39
40
41 730 Granger, Darryl E. 2006. “A Review of Burial Dating Methods Using ^{26}Al and ^{10}Be .” *Special*
42
43 731 *Paper 415: In Situ-Produced Cosmogenic Nuclides and Quantification of Geological*
44
45 732 *Processes* 2415 (01): 1–16. [https://doi.org/10.1130/2006.2415\(01\)](https://doi.org/10.1130/2006.2415(01)).
46
47
48
49 733 Jackson, James, & Dan Mckenzie. 1988. “The Relationship between Plate Motions and Seismic
50
51 734 Moment Tensors, and the Rates of Active Deformation in the Mediterranean and Middle
52
53 735 East.” *Geophysical Journal* 93: 45–73.
54
55
56
57
58
59
60

- 1
2
3 736 Jackson, J. 1992. "Partitioning of Strike-Slip and Convergent Motion between Eurasia and Arabia
4
5
6 737 in Eastern Turkey and the Caucasus." *Journal of Geophysical Research* 97 (B9): 12471–79.
7
8 738 <https://doi.org/10.1016/j.cardfail.2009.04.002>.
9
10
11 739 JAXA. 2017. "ALOS Global Digital Surface Model (DSM) ' ALOS World 3D-30m ' (AW3D30)
12
13
14 740 Dataset Product Format Description Earth Observation Research Center (EORC), Japan
15
16 741 Aerospace Exploration Agency (JAXA)," no. March: 11.
17
18
19 742 Jones, R. W., & M. D. Simmons. 1996. "A Review of the Stratigraphy of Eastern Paratethys
20
21
22 743 (Oligocene-Holocene)." *Bulletins of Natural History Museum of London* 52 (27): 25–49.
23
24
25 744 Keller, E. A., Larry Gurrola, & T. E. Tierney. 1999. "Geomorphic Criteria to Determine Direction
26
27 745 of Lateral Propagation of Reverse Faulting and Folding." *Geology* 27 (6): 515–18.
28
29
30 746 [https://doi.org/10.1130/0091-7613\(1999\)027<0515:GCTDDO>2.3.CO;2](https://doi.org/10.1130/0091-7613(1999)027<0515:GCTDDO>2.3.CO;2).
31
32
33 747 Kereselidze, K. 1950. "Alazani Artesian Basin (In Russian)." Tbilisi.
34
35
36 748 Kirby, E, & Kelin X. Whipple. 2001. "Quantifying Rockuplift Rates via Stream pro Le Analysis."
37
38 749 *Geology* 29 (5): 415–18. [https://doi.org/10.1130/0091-](https://doi.org/10.1130/0091-7613(2001)029<0415:QDRURV>2.0.CO;2)
39
40
41 750 [7613\(2001\)029<0415:QDRURV>2.0.CO;2](https://doi.org/10.1130/0091-7613(2001)029<0415:QDRURV>2.0.CO;2).
42
43
44 751 Kirby, Eric, Kelin X. Whipple, Wenqing Tang, & Zhiliang Chen. 2003. "Distribution of Active Rock
45
46 752 Uplift along the Eastern Margin of the Tibetan Plateau: Inferences from Bedrock Channel
47
48 753 Longitudinal Profiles." *Journal of Geophysical Research: Solid Earth* 108 (B4).
49
50
51 754 <https://doi.org/10.1029/2001JB000861>.
52
53
54 755 Kirby, Eric, & Kelin X Whipple. 2012. "Expression of Active Tectonics in Erosional Landscapes."
55
56
57
58
59
60

- 1
2
3 756 *Journal of Structural Geology* 44: 54–75. <https://doi.org/10.1016/j.jsg.2012.07.009>.
4
5
6 757 Kohl, C. P., & K. Nishiizumi. 1992. “Chemical Isolation of Quartz for Measurement of In-Situ -
7
8
9 758 Produced Cosmogenic Nuclides.” *Geochimica et Cosmochimica Acta* 56 (9): 3583–87.
10
11 759 [https://doi.org/10.1016/0016-7037\(92\)90401-4](https://doi.org/10.1016/0016-7037(92)90401-4).
12
13
14 760 W. Krijgsman, A. Tesakov, T. Yanina, S. Lazarev, G. Danukalova, C.G.C. Van Baak, J. Agustí, M.C.
15
16 761 Alçiçek, E. Aliyeva, D. Bista, A. Bruch, Y. Büyükmeriç, M. Bukhsianidze, R. Flecker, P. Frolov,
17
18 762 T.M. Hoyle, E.L. Jorissen, U. Kirscher, S.A. Koriche, S.B. Kroonenberg, D. Lordkipanidze, O.
19
20 763 Oms, L. Rausch, J. Singarayer, M. Stoica, S. van de Velde, V.V. Titov, & F.P. Wesselingh.
21
22 764 2018. “Quaternary Time Scales for the Pontocaspian Domain: Interbasinal Connectivity and
23
24 765 Faunal Evolution.” *Earth-Science Reviews* 188: 1–40.
25
26 766 <https://doi.org/10.1016/j.earscirev.2018.10.013>.
27
28
29 767 Krijgsman. 2019. “Magneto-Biostratigraphic Age Constraints on the Palaeoenvironmental
30
31 768 Evolution of the South Caspian Basin during the Early-Middle Pleistocene (Kura Basin,
32
33 769 Azerbaijan).” *Quaternary Science Reviews* 222 (September): 105895.
34
35 770 <https://doi.org/10.1016/j.quascirev.2019.105895>.
36
37
38
39 771 Lague, Dimitri. 2014. “The Stream Power River Incision Model: Evidence, Theory and Beyond.”
40
41 772 *Earth Surface Processes and Landforms* 39 (1): 38–61. <https://doi.org/10.1002/esp.3462>.
42
43
44
45 773 Lawton, Timothy F, Steven E Boyer, & James G Schmitt. 1994. “And Conglomerate Distribution ,
46
47 774 Cordilleran Fold.” *Geology* 22: 339–42.
48
49
50
51 775 Lazarev, Sergei, Elisabeth L. Jorissen, Sabrina van de Velde, Lea Rausch, Marius Stoica, Frank P.
52
53
54
55
56
57
58
59
60

- 1
2
3 776 Wesselingh, Christiaan G.C. Van Baak, Tamara A. Yanina, Elmira Aliyeva, a Wout
4
5
6 777 Merritts, Dorothy J, Kirk R Vincent, \$ Ellen E Wohl. 1994. "Long River Profiles, Tectonism, and
7
8
9 778 Eustasy: A Guide to Interpreting Fluvial Terraces." *Journal of Geophysical Research* 99:
10
11 779 14031–50.
12
13
14 780 Miao, Xiaodong, Huayu Lu, Zhen Li, & Guangchao Cao. 2008. "Paleocurrent and Fabric Analyses
15
16
17 781 of the Imbricated Fluvial Gravel Deposits in Huangshui Valley, the Northeastern Tibetan
18
19 782 Plateau, China." *Geomorphology* 99 (1–4): 433–42.
20
21
22 783 <https://doi.org/10.1016/j.geomorph.2007.12.005>.
23
24
25 784 Mifsud, Charles, Toshiyuki Fujioka, & David Fink. 2013. "Extraction and Purification of Quartz in
26
27 785 Rock Using Hot Phosphoric Acid for in Situ Cosmogenic Exposure Dating." *Nuclear*
28
29 786 *Instruments and Methods in Physics Research, Section B: Beam Interactions with Materials*
30
31
32 787 *and Atoms* 294: 203–7. <https://doi.org/10.1016/j.nimb.2012.08.037>.
33
34
35 788 Mitchell, Nate A., & Brian J. Yanites. 2019. "Spatially Variable Increase in Rock Uplift in the
36
37 789 Northern U.S. Cordillera Recorded in the Distribution of River Knickpoints and Incision
38
39
40 790 Depths." *Journal of Geophysical Research: Earth Surface* 124 (5): 1238–60.
41
42
43 791 <https://doi.org/10.1029/2018JF004880>.
44
45
46 792 Montgomery, David R., & Mark T. Brandon. 2002. "Topographic Controls on Erosion Rates in
47
48 793 Tectonically Active Mountain Ranges." *Earth and Planetary Science Letters* 201 (3–4): 481–
49
50 794 89. [https://doi.org/10.1016/S0012-821X\(02\)00725-2](https://doi.org/10.1016/S0012-821X(02)00725-2).
51
52
53 795 Mosar, Jon, Talat Kangarli, Martin Bochud, Ulrich A. Glasmacher, Annick Rast, Marie-Francoise
54
55
56
57
58
59
60

- 1
2
3 796 Brunet, & Marc Sosson. 2010. "Cenozoic-Recent Tectonics and Uplift in the Greater
4
5 797 Caucasus: A Perspective from Azerbaijan." *Geological Society, London, Special Publications*
6
7 798 340 (1): 261–80. <https://doi.org/10.1144/SP340.12>.
8
9
10
11 799 Nichols, Gary. 2009. *Sedimentology and Stratigraphy. 2nd Edition*. John Wiley & Sons Ltd.,
12
13
14 800 Onur, T, Gok, R, Godoladze, T, Gunia, I, Boichenko, G, Buzaladze, A, Tumanova, N, Dzmanashvili,
15
16 801 M, Sukhishvili, L, Javakishvili, Z, Cowgill, E, Bondar, I, & Yetirmishli, G. 2019.
17
18 802 "PROBABILISTIC SEISMIC HAZARD ASSESSMENT FOR GEORGIA." *Lawrence Livermore*
19
20 803 *National Lab. (LLNL), Livermore, CA (United States)*. <https://doi.org/10.2172/1511856>.
21
22
23
24 804 Reilinger, Robert, McClusky, Simon Vernant, Philippe Lawrence, Shawn Ergintav, Semih Cakmak,
25
26 805 Rahsan Ozener, Haluk Kadirov, Fakhraddin Guliev, Ibrahim Stepanyan, Ruben Nadariya,
27
28 806 Merab Hahubia, Galaktion Mahmoud, Salah Sakr, K. ArRajehi, Abdullah Paradissis, Demitris
29
30 807 Al-Aydrus, A. Prilepin, Mikhail Guseva, Tamara Evren, Emre Dmitrotsa, Andriy Filikov, S. V.
31
32 808 Gomez, Francisco Al-Ghazzi & Riad Karam, Gebran. 2006. "GPS Constraints on Continental
33
34 809 Deformation in the Africa-Arabia-Eurasia Continental Collision Zone and Implications for
35
36 810 the Dynamics of Plate Interactions." *Journal of Geophysical Research: Solid Earth* 111 (5):
37
38 811 1–26. <https://doi.org/10.1029/2005JB004051>.
39
40
41
42 812 Rossi, Matthew W., Mark C. Quigley, John M. Fletcher, Kelin X. Whipple, J. Jesús Díaz-Torres,
43
44 813 Christian Seiler, L. Keith Fifield, & Arjun M. Heimsath. 2017. "Along-Strike Variation in
45
46 814 Catchment Morphology and Cosmogenic Denudation Rates Reveal the Pattern and History
47
48 815 of Footwall Uplift, Main Gulf Escarpment, Baja California." *Bulletin of the Geological*
49
50 816 *Society of America* 129 (7–8): 837–54. <https://doi.org/10.1130/B31373.1>.
51
52
53
54
55
56
57
58
59
60

- 1
2
3 817 Schwanghart, W., & D. Scherler. 2014. "Short Communication: TopoToolbox 2 - MATLAB-Based
4
5 818 Software for Topographic Analysis and Modeling in Earth Surface Sciences." *Earth Surface*
6
7
8 819 *Dynamics* 2 (1): 1–7. <https://doi.org/10.5194/esurf-2-1-2014>.
9
10
11 820 Sidorenko, A, & P Gamkrelidze, eds. 1964. "Geology of USSR." In *SSSR Geology (In Russian)*, 1–
12
13 821 648. Moscow.
- 14
15
16
17 822 Snyder, Noah P, Kelin X. Whipple, Gregory E Tucker, Dorothy J Merritts, & Marshall College.
18
19 823 2000. "Stream Profiles in the Mendocino Triple Junction Region , Northern California."
20
21 824 *Geological Society of America Bulletin* 112 (8): 1250–63. <https://doi.org/10.1130/0016->
22
23 825 [7606\(2000\)112<1250:lrrtfd>2.3.co;2](https://doi.org/10.1130/0016-7606(2000)112<1250:lrrtfd>2.3.co;2).
- 24
25
26
27 826 Sokhadze, G., M. Floyd, T. Godoladze, R. King, E. S. Cowgill, Z. Javakhishvili, G. Hahubia, & R.
28
29 827 Reilinger. 2018. "Active Convergence between the Lesser and Greater Caucasus in Georgia:
30
31 828 Constraints on the Tectonic Evolution of the Lesser–Greater Caucasus Continental
32
33 829 Collision." *Earth and Planetary Science Letters* 481: 154–61.
34
35 830 <https://doi.org/10.1016/j.epsl.2017.10.007>.
- 36
37
38
39
40 831 Tadono, T., H. Nagai, H. Ishida, F. Oda, S. Naito, K. Minakawa, & H. Iwamoto. 2016. "Generation
41
42 832 of the 30 M-MESH Global Digital Surface Model by Alos Prism." *International Archives of*
43
44 833 *the Photogrammetry, Remote Sensing and Spatial Information Sciences - ISPRS Archives* 41
45
46 834 (July): 157–62. <https://doi.org/10.5194/isprsarchives-XLI-B4-157-2016>.
- 47
48
49
50 835 Tan, O, & T Taymaz. 2006. "Active Tectonics of the Caucasus: Earthquake Source Mechanisms
51
52 836 and Rupture Histories Obtained from Inversion of Teleseismic Body Waveforms."
53
54 837 *Postcollisional Tectonics and Magmatism in the Mediterranean Region and Asia* 409 (25):
55
56
57
58
59
60

- 1
2
3 838 531-578\631. [https://doi.org/10.1130/2006.2409\(25\)](https://doi.org/10.1130/2006.2409(25)).
4
5
6 839 Vermeesch, Pieter. 2007. "CosmoCalc: An Excel Add-in for Cosmogenic Nuclide Calculations."
7
8
9 840 *Geochemistry, Geophysics, Geosystems* 8 (8): 1–14.
10
11 841 <https://doi.org/10.1029/2006GC001530>.
12
13
14 842 Vincent, Stephen J., William Braham, Vladimir A. Lavrishchev, James R. Maynard, & Melise
15
16
17 843 Harland. 2016. "The Formation and Inversion of the Western Greater Caucasus Basin and
18
19 844 the Uplift of the Western Greater Caucasus: Implications for the Wider Black Sea Region."
20
21 845 *Tectonics* 35 (12): 2948–62. <https://doi.org/10.1002/2016TC004204>.
22
23
24 846 Whipple, Kelin X. 2004. "Bedrock Rivers and the Geomorphology of Active Orogens." *Annual*
25
26
27 847 *Review of Earth and Planetary Sciences* 32 (1): 151–85.
28
29 848 <https://doi.org/10.1146/annurev.earth.32.101802.120356>.
30
31
32 849 Whipple, Kelin X. 2009. "The Influence of Climate on the Tectonic Evolution of Mountain Belts."
33
34
35 850 *Nature Geoscience* 2 (2): 97–104. <https://doi.org/10.1038/ngeo413>.
36
37
38 851 Whittaker, Alexander C. 2012. "How Do Landscapes Record Tectonics and Climate?"
39
40
41 852 *Lithosphere* 4 (2): 160–64. <https://doi.org/10.1130/RF.L003.1>.
42
43
44 853 Whittaker, Alexander C., & Sarah J. Boulton. 2012. "Tectonic and Climatic Controls on
45
46 854 Knickpoint Retreat Rates and Landscape Response Times." *Journal of Geophysical*
47
48
49 855 *Research: Earth Surface* 117 (2): 1–19. <https://doi.org/10.1029/2011JF002157>.
50
51
52 856 Wobus, C, K X Whipple, E Kirby, N Snyder, J Johnson, K Spyropolou, B Crosby, & D Sheehan.
53
54 857 2006. "Tectonics from Topography: Procedures, Promise, and Pitfalls." *Geological Society*
55
56
57
58
59
60

1
2
3
4
5
6
7
8
9
10
11
12
13
14
15
16
17
18
19
20
21
22
23
24
25
26
27
28
29
30
31
32
33
34
35
36
37
38
39
40
41
42
43
44
45
46
47
48
49
50
51
52
53
54
55
56
57
58
59
60

858 *of America Special Paper* 398 (04): 55–74. [https://doi.org/10.1130/2006.2398\(04\)](https://doi.org/10.1130/2006.2398(04)).

Proof For Review

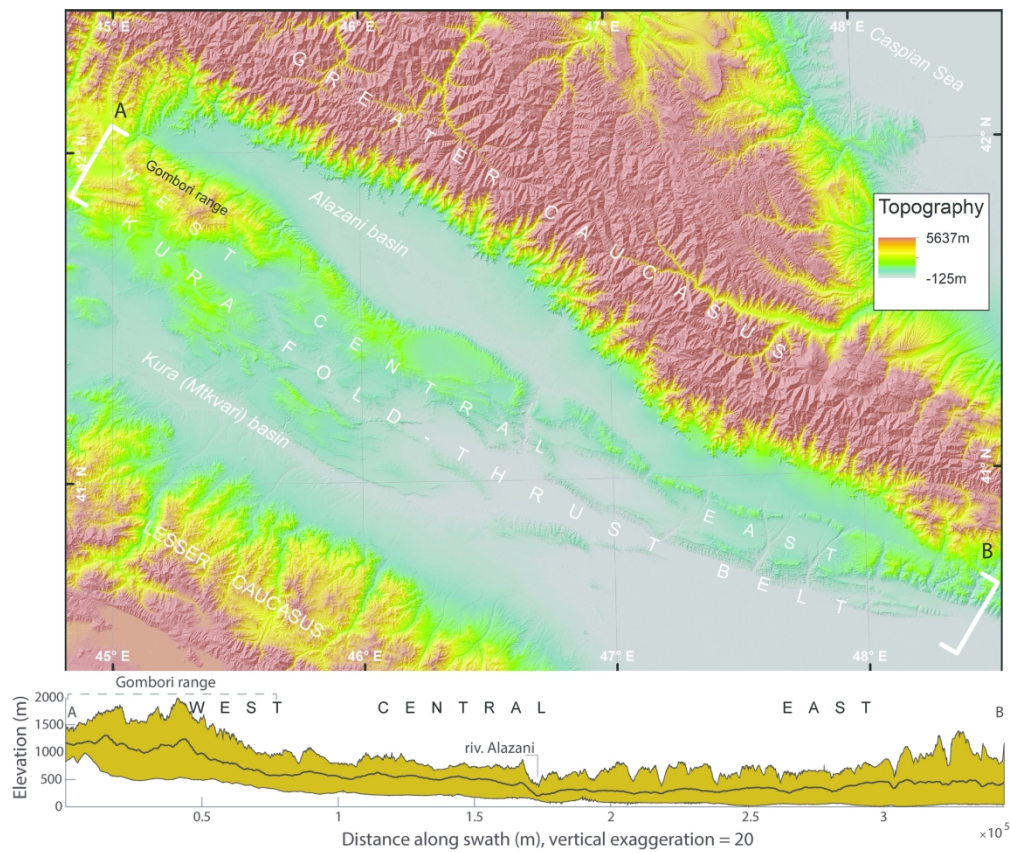


Figure 1. Location and topography of KFTB

168x141mm (300 x 300 DPI)

1
2
3
4
5
6
7
8
9
10
11
12
13
14
15
16
17
18
19
20
21
22
23
24
25
26
27
28
29
30
31
32
33
34
35
36
37
38
39
40
41
42
43
44
45
46
47
48
49
50
51
52
53
54
55
56
57
58
59
60

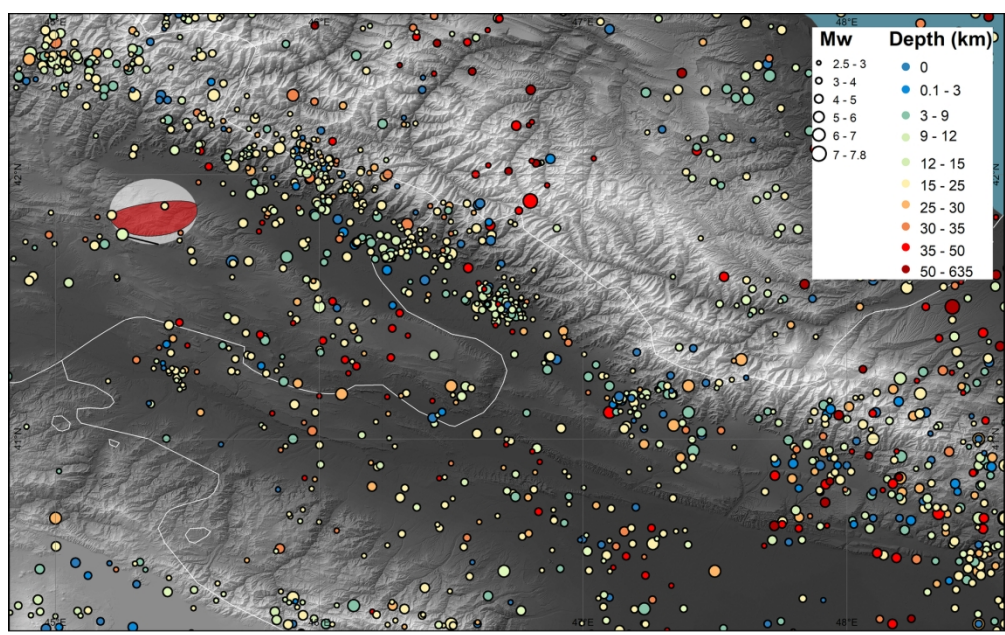


Figure 2. Earthquake events of KFTB from Complete Catalogue of Instrumental Seismicity for Georgia (Onur *et al.* 2019), fault plane solution by (Tan & Taymaz, 2006)

168x104mm (300 x 300 DPI)

Period	Epoch	Stage	Suite	Thickness (m)	Lithology
Quaternary		Upper Pleistocene - Holocene		50	
	Pleistocene	Middle pleistocene	Alazani suite 3	200	Cobble, conglomerate, loam and clay
	Pleistocene	Calabrian	Alazani suite 2	400	Loam, clay, cobble and conglomerate
Neogene - Quaternary	Pliocene - Pleistocene	Gelasian- Middle Pleistocene	Akchagylian- Apsheronian, Alazani suite 1	1200	Conglomerate, cobble, loam and clay
Neogene	Miocene	Tortonian-Messinian	Meotian-Pontian	1500	Upper: Conglomerates, Lower: sandstone and clay deposit
Paleogene	Eocene and Oligocene	Priabonian-Rupelian	Kint	350+115	Clay with sandstone layers + arkosic and arkosic-greywacke sandstone and clay
Lower and Upper Cretaceous	Upper	Upper Turonian	Margalitis klde	65	Limestone, marl and clay
	Upper	Upper Cenomanian, Lower Turonian	Ananuri	50	Claystone and marl
	Upper	Cenomanian	Ukugmarti	150	Sandstone, limestone and claystone
	Lower	Albian	Navtskhevi	150	Clay, marl, claystone and sandstone
	Lower	Aptian	Tempakhevi	300	Clay, claystone, sandstone, marl, limestone

Figure 3. Stratigraphy of the Gombori range compiled after (Buleishvili, 1974), (Zedginidze *et al.* 1971), (Kereselidze, 1950), (Sidorenko & Gamkrelidze, 1964), (Buachidze *et al.* 1950). Thicknesses are approximate and likely vary along-strike within the Gombori Range

168x117mm (600 x 600 DPI)

1
2
3
4
5
6
7
8
9
10
11
12
13
14
15
16
17
18
19
20
21
22
23
24
25
26
27
28
29
30
31
32
33
34
35
36
37
38
39
40
41
42
43
44
45
46
47
48
49
50
51
52
53
54
55
56
57
58
59
60

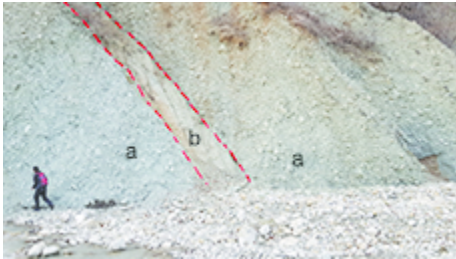


Figure 4. Base of Al₁ series from catchment 7, view to the NW showing steeply, NE dipping conglomeratic (a) and sandy loam (b) beds

80x45mm (72 x 72 DPI)



Figure 5. NE dipping volcanic ash layer exposed in catchment 12, facies 2

80x34mm (300 x 300 DPI)

1
2
3
4
5
6
7
8
9
10
11
12
13
14
15
16
17
18
19
20
21
22
23
24
25
26
27
28
29
30
31
32
33
34
35
36
37
38
39
40
41
42
43
44
45
46
47
48
49
50
51
52
53
54
55
56
57
58
59
60

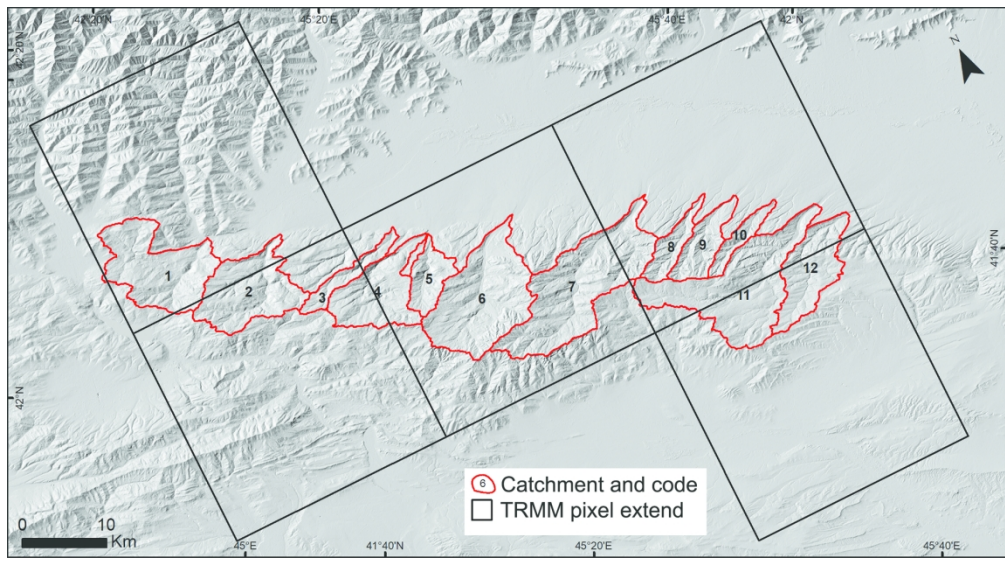


Figure 6. TRMM 3B42 pixel extends (black) and catchments of the study area (red) and the identifying numbers for those catchments referenced in the text

80x44mm (600 x 600 DPI)

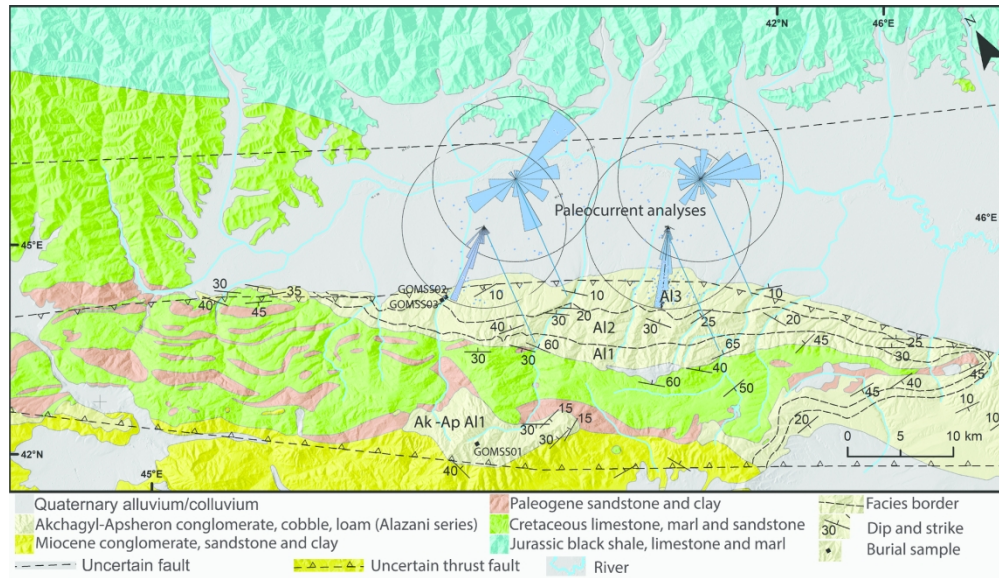


Figure 7. Simplified lithology, sampling sites and paleocurrent directions

168x97mm (300 x 300 DPI)

1
2
3
4
5
6
7
8
9
10
11
12
13
14
15
16
17
18
19
20
21
22
23
24
25
26
27
28
29
30
31
32
33
34
35
36
37
38
39
40
41
42
43
44
45
46
47
48
49
50
51
52
53
54
55
56
57
58
59
60

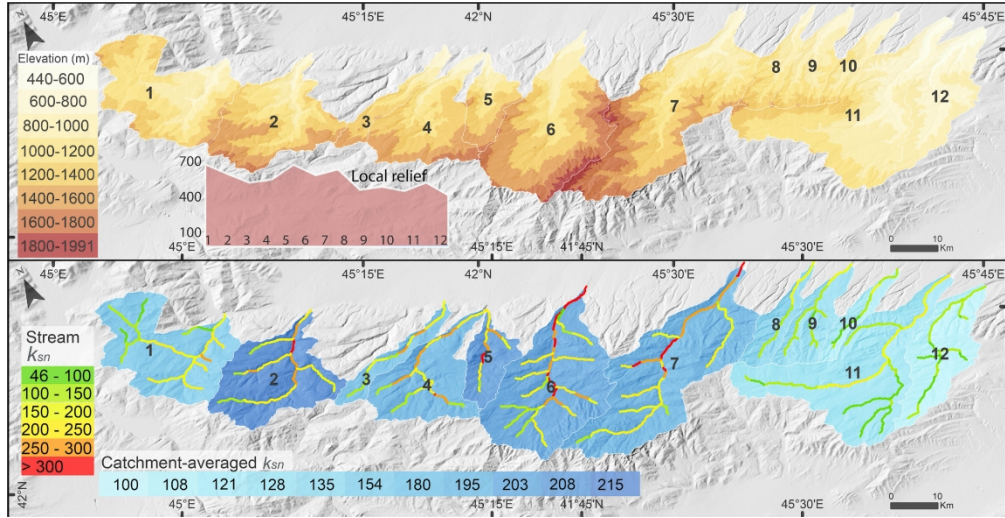


Figure 8. Topography and local relief maps of catchments (upper). Catchment averaged and stream k_{sn} values (below). See text for details of these calculations

169x87mm (600 x 600 DPI)

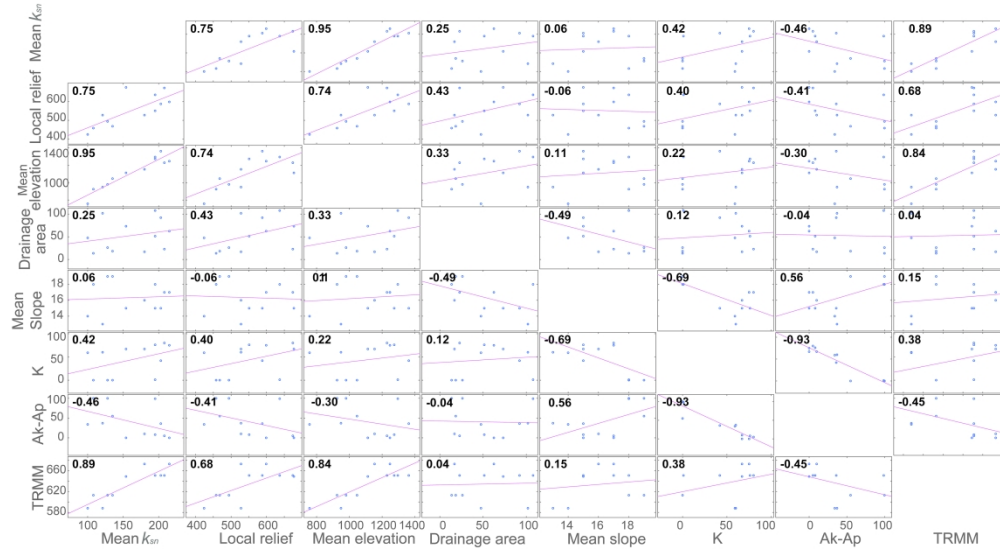


Figure 9. correlation matrix of different indices. Units: Local relief – meter; Mean elevation – meter; Mean slope – degree; K (Cretaceous rocks) – Percentage of catchment covered by these rocks; AkAp (Akchagyl-Apsheron) – Percentage of catchment covered by these rocks; TRMM – millimeter/annual mean

168x93mm (600 x 600 DPI)

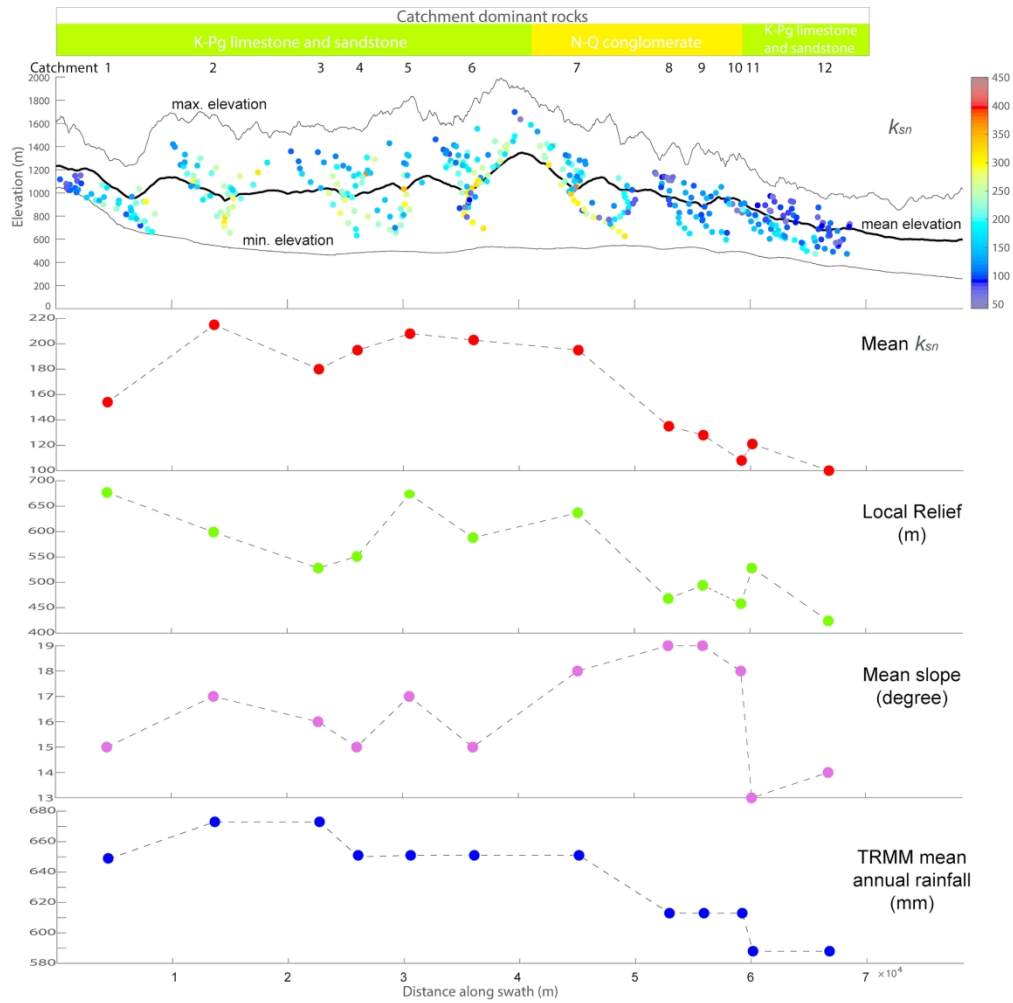


Figure 10. Swath profile of topography, k_{sn} values (upper graph) and along swath geomorphologic indices and rainfall data

168x167mm (300 x 300 DPI)

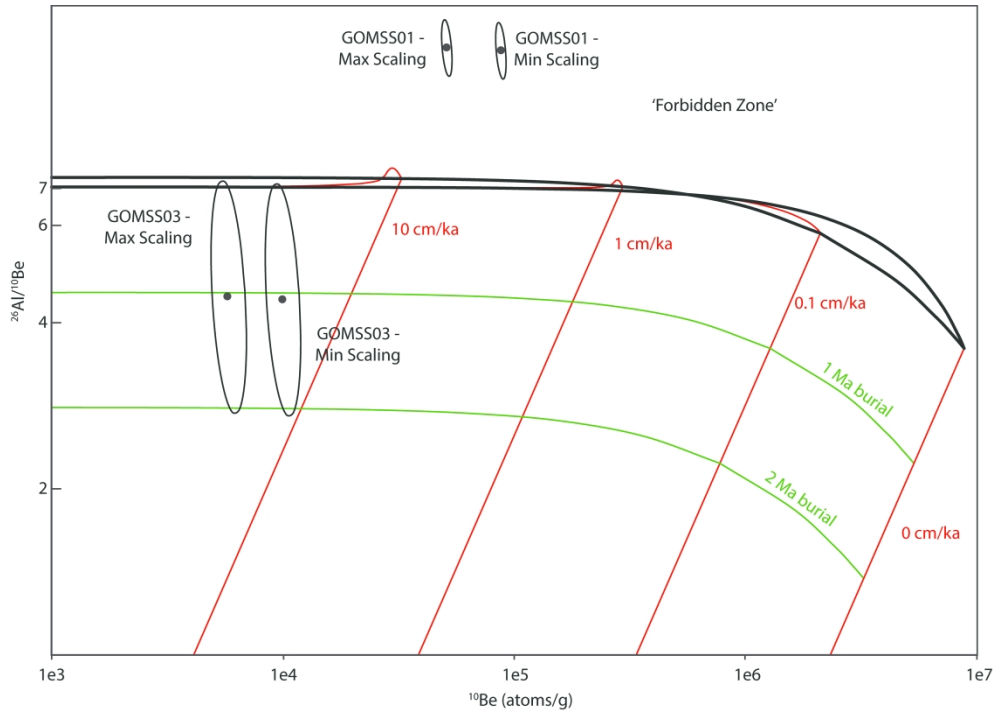
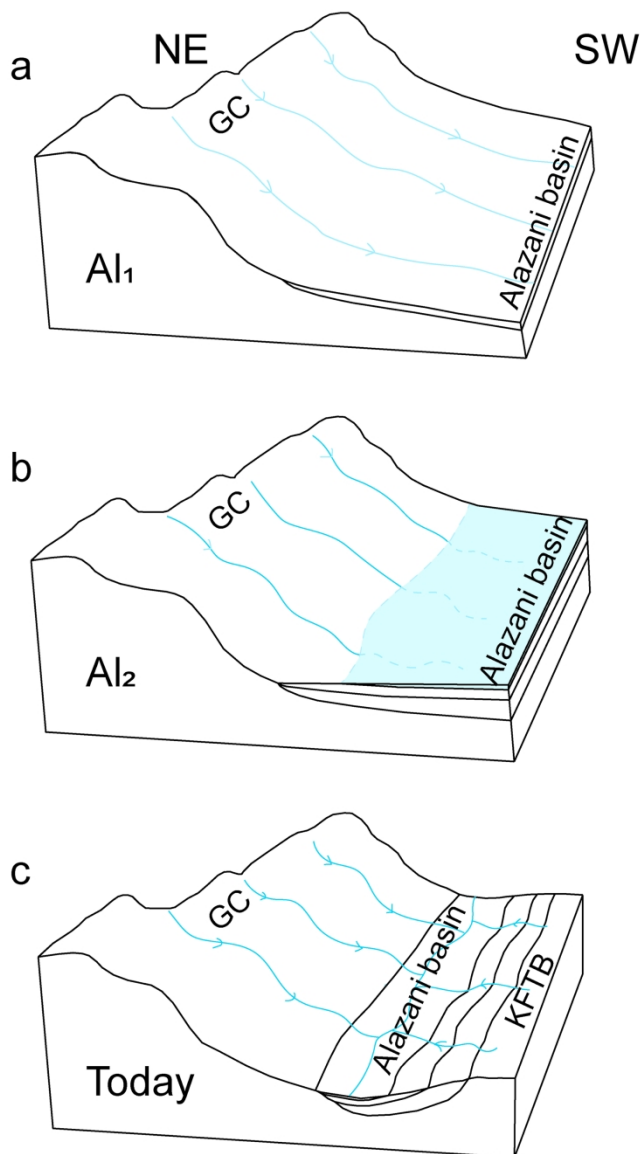


Figure 11. Erosion island plot for Gombori range samples. Variability in production rate scaling for the two samples, GOMSS01 and GOMSS03 are reflected in the pairs of points. Sample GOMSS01 plots in the forbidden zone and are thus interpretable. Sample GOMSS03 have mean ages of ~ 1 Ma regardless of exact scaling relationships used. The relatively high uncertainties on the ages reflect high native Al concentrations. Burial isochrons are reported in Ma and bounds for estimated paleo erosion rates in cm/ka. Plots produced using CosmoCalc (Vermeesch, 2007)

168x119mm (600 x 600 DPI)



45 Figure 12. Fluvial system evolution diagram for the western KFTB. A) During the deposition of Alazani
46 Suite1 (Al₁), rivers draining from the Greater Caucasus were still able to flow directly south across what is
47 now the KFTB. B) Alazani Suite 2 (Al₂) represents deposition in a lacustrine setting, which could relate to
48 damming of rivers by growth of the KFTB, or could be related to broader, basin wide changes in base-level.

49 C) By the time of deposition of Alazani Suite 3 (Al₃), the river network in the northwestern KFTB had
50 developed into something similar to the modern, with rivers draining northward out of the Gombori range
51 and with a well-defined axial drainage occupying the Alazani basin

52 80x135mm (600 x 600 DPI)

53
54
55
56
57
58
59
60

Geological Magazine

Active deformation and Plio-Pleistocene fluvial reorganization of the western Kura Fold-Thrust Belt, Georgia: implications for the evolution of the Greater Caucasus mountains and seismic hazard

Lasha Sukhishvili,

Adam M. Forte,

Giorgi Merebashvili,

Joel Leonard,

Kelin X. Whipple,

Zurab Javakhishvili,

Arjun Heimsath,

Tea Godoladze

Supplementary Material

Proof For Review

1
2
3
4
5
6
7
8
9
10
11
12
13
14
15
16
17
18
19
20
21
22
23
24
25
26
27
28
29
30
31
32
33
34
35
36
37
38
39
40
41
42
43
44
45
46
47

Supplementary Table S1. Sample information for the three samples analyzed for burial-age dating

Sample ID	Latitude (°N)	Longitude (°E)	Elevation (m)	Quartz mass (g)	Mass ⁹ Be (g)	Mass ²⁷ Al (g)	¹⁰ Be/ ⁹ Be ±	²⁶ Al/ ²⁷ Al ±	¹⁰ Be (atoms/g) ±	²⁶ Al (atoms/g) ±
GOMSS01	41.80815	45.34789	1831	49.7598	4.91E-04	4.8546E-02	2.8825E-13 ± 6.7986E-15	1.0655E-13 ± 5.5598E-15	1.88E+05 ± 4.87E+03	2.32E+06 ± 1.23E+05
GOMSS02	41.92953	45.40144	749	NA	NA	NA	NA	NA	NA	NA
GOMSS03	41.928925	45.395784	768	71.5252	4.88E-04	3.8899E-02	4.974E-14 ± 4.0645E-15	7.5273E-15 ± 1.7049E-15	2.12E+04 ± 1.87E+03	9.14E+04 ± 2.07E+04

Proof For Review

Supplementary Table S1. Parameters used for the four different scaling schemes for calculating production rates of ^{26}Al and ^{10}Be for interpreting the burial age dating, see text for more detail

Production site	Latitude	Longitude	Elevation	Rc (GV)	Atmospheric depth (g/cm ²)	Desilets et al 2006 ^{10}Be scaling	Desilets et al 2006 ^{26}Al scaling	Burial age (Ma)	2.5 Percentile (Ma)	97.5 Percentile (Ma)
'Local'	42.336	44.80	1858.2	4.74	825	4.25	4.22	9.77E-01	4.84E-03	2.53E+00
'Avgari'	42.1182	45.02	1226.2	4.81	892	2.57	2.56	1.01E+00	7.93E-03	2.62E+00
'Iori'	42.1942	45.4762	1226.2	4.79	903	2.37	2.36	1.02E+00	1.53E-02	2.59E+00
'SE GC'	41.8657	45.3458	1472.6	4.90	865	3.12	3.10	9.76E-01	3.80E-03	2.23E+00